Clin Rheumatol
DOI 10.1007/s10067-009-1358-x

CASE REPORT

# Successful treatment with tacrolimus of progressive interstitial pneumonia associated with amyopathic dermatomyositis refractory to cyclosporine

**Masaru Ando · Eishi Miyazaki · Mari Yamasue · Yukiko Sadamura · Toshihiro Ishii · Ryuichi Takenaka · Takeo Ito · Shin-ichi Nureki · Toshihide Kumamoto**

Received: 2 October 2009 / Accepted: 21 December 2009


**Abstract** A 58-year-old male was admitted to our hospital because of periungual nailfold an erythema and erythematous rash on the dorsal joints of his hands and feet, but no muscle weakness. He was thus diagnosed to have amyopathic dermatomyositis. He had moderate hypoxemia and his chest computed tomography scans demonstrated bilateral ground-glass opacities, implicating complication with interstitial pneumonia. Therapy was initiated with pulsed methylprednisolone followed by high-dose corticosteroids, pulsed cyclophosphamide, and cyclosporine. The skin manifestations improved; however, the pulmonary infiltrates and hypoxemia deteriorated during the 2-month period of the treatment. The treatment was switched from cyclosporine to tacrolimus because of an inadequate clinical response to the therapy, and this resulted in the resolution of interstitial pneumonia. This case indicates that tacrolimus administration should be considered for patients with this life-threatening disorder when it is judged to be refractory to cyclosporine.

**Keywords** Amyopathic dermatomyositis · Interstitial pneumonia · Tacrolimus

## Introduction

Progressive interstitial pneumonia associated with amyopathic dermatomyositis (ADM) has been reported to show poor a response to therapy and has high mortality [1]. Recent reports suggest that early administration of cyclosporine for this life-threatening condition provides a favorable prognosis for some patients, but not for all [2–5]. This report presents a case with progressive interstitial pneumonia associated with ADM refractory to a combination therapy with high-dose corticosteroids, pulsed cyclophosphamide, and cyclosporine, in which a switch from cyclosporine to tacrolimus resulted in the resolution of the interstitial pneumonia.

## Case report

A 58-year-old male was admitted because of a 1 month history of dyspnea on effort, general fatigue, low grade fever, and rashes, including periungual nailfold erythema, Gottron's papules on the metacarpophalangeal joints, and erythema around the elbow and knee joints. A deep skin biopsy showed a perivascular inflammatory infiltrate containing numerous lymphocytes in the upper dermis, consistent with the characteristic histopathological changes associated with dermatomyositis. The white blood cell count was 15,300/μl with 89.2% neutrophils and C-reactive protein level was 0.68 mg/dl (<0.21 mg/dl). The antinuclear antibody titer was elevated (×160), but anti-histidyl-tRNA synthetase antibodies (anti-Jo-1) were not detected. The creatine kinase level was slightly elevated (502 IU/L: 62–287 IU/L) and the aldorase was normal (5.2 IU/L: 2.1–6.1 IU/L). No muscle weakness was noted, and electromyography did not detect any abnormal wave. No myositis was detected in the muscle biopsy specimens obtained from the biceps. Therefore, ADM was diagnosed based on the criteria by Sontheimer [1].

He had experienced exertional dyspnea for a month. Fine crackles were audible bilaterally. An arterial blood gas analysis revealed pH of 7.381, $PaO_2$ of 65.3 Torr, and

M. Ando (✉) · E. Miyazaki · M. Yamasue · Y. Sadamura · T. Ishii · R. Takenaka · T. Ito · S.-i. Nureki · T. Kumamoto
Department of Internal Medicine 3,
Oita University Faculty of Medicine,
Idaigaoka 1-1, Hasama,
Yufu, Oita 879-5593, Japan
e-mail: mando@med.oita-u.ac.jp

Published online: 04 February 2010

$PaCO_2$ of 40.7 Torr. The circulating level of KL-6, a marker of interstitial pneumonia, was elevated with a value of 1,300 U/ml (<500 U/ml). A chest roentgenogram revealed faint reticular shadow in both lower lung fields. Chest high-resolution computed tomography (HRCT) scans showed bilateral subpleural reticular opacity with ground-glass attenuation (Fig. 1a). Bronchoalveolar lavage fluid (BALF) contained $2.93 \times 10^5$ cells/ml with 31.3% lymphocytes and 19.3% neutrophils. A CD4/CD8 ratio was 0.98. Cultures of blood, urine, and BALF to detect bacteria, fungi, and mycobacteria were negative and serological tests for atypical pathogens including *Mycoplasma pneumoniae*, *Clamydia pneumoniae*, and *Legionella* were negative as were β-D glucan and cytomegalovirus antigenemia.

The patient was thus diagnosed to have interstitial pneumonia associated with ADM, and therapy was initiated with methylprednisolone pulse-therapy (1 g/day, intravenously for 3 days) followed by high-dose oral prednisolone (60 mg/day), cyclosporine, and monthly pulsed cyclophosphamide (500 mg, intravenously). A trough value of cyclosporine was maintained between 100 and 150 ng/ml. The administration of this treatment regimen for 2 months, improved the skin manifestations; however, the chest images gradually deteriorated with lung shrinkage in chest roentgenograms and increased ground-glass opacities with patchy consolidation in HRCT scans (Fig. 1b). Because of the progressive hypoxemia, the patient was forced to receive high-dose oxygen. The interstitial pneumonia was judged to be refractory to the combination therapy including cyclosporine; therefore, the decision was made to switch the immunosuppressant from cyclosporine to tacrolimus with the minimum serum levels maintained between 5–10 ng/ml. This resulted in the gradual improvement of arterial blood gasses and the infiltrates in chest images. The lung opacities were almost resolved after the 9 months of tacrolimus administration, when prednisolone was tapered to 17.5 mg daily (Fig. 1c), and oxygen inhalation was not needed even on exercise. The patient experienced a cytomegalovirus infection as an adverse event during the course of combination therapy including tacrolimus. The infection was diagnosed based on the detection of the virus by antigenemia and it was successfully treated with ganciclovir.

## Discussion

Interstitial pneumonia associated with ADM often shows aggressive course leading to death [2]. The early administration of cyclosporine in combination with high-dose corticosteroids is usually capable of decreasing the mortality in this fatal complication of ADM [3, 4]; however, numerous patients have died of respiratory failure despite early administration of cyclosporine [5, 6]. In this case, a switch of the immunosuppressant from cyclosporine to tacrolimus resulted in the resolution of interstitial pneumonia. This is the first reported case of a patient being rescued by using tacrolimus for progressive interstitial pneumonia associated with ADM, which was resistant to the conventional immunosuppressive therapies.

The lymphocyte number in the BALF was increased in this patient, similar to that reported in the previous papers [3–5]. Therefore, activated T lymphocytes may play a role in the pathogenesis of ADM as well as classical dermatomyositis; therefore, cyclosporine, a potent T-cell inhibitor, is employed for the treatment of progressive interstitial

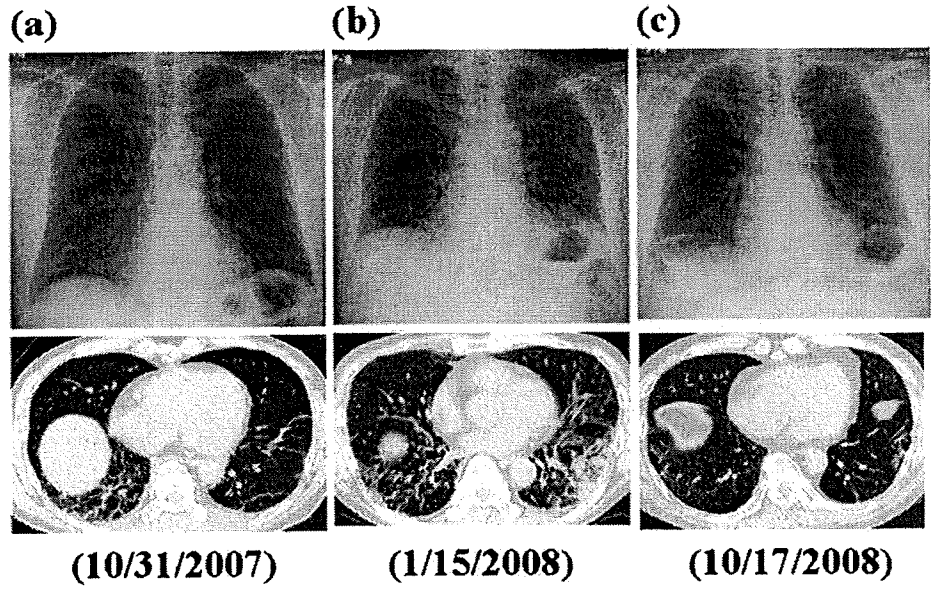


**Fig. 1** **a** A chest roentgenogram on admission shows a faint reticular shadow in bilateral lower lung fields. Chest high-resolution computed tomography scans show bilateral subpleural reticular opacities with ground-glass attenuation. **b** A chest roentgenogram reveals increased reticular shadows with lung shrinkage during the 2 months of combination therapy including cyclosporine and the chest HRCT scans also show increased ground-glass opacities with patchy consolidation. **c** A chest roentgenogram and chest HRCT scans 9 months after the administration of tacrolimus show dramatic improvement of pulmonary infiltrates and shrinkage of the lung

pneumonia associated with ADM. However, previous papers disclosed that the efficacy of cyclosporine is limited [5, 6]. In this patient, a switch from cyclosporine to tacrolimus led to rescue the patient, indicating that tacrolimus may be superior to cyclosporine. Tacrolimus is a macrolide immunosuppressant with actions similar to those of cyclosporine, but the potency of tacrolimus in inhibiting in vitro T-cell activation and proliferation is up to 100 times greater than that of cyclosporine [7]. Although cyclosporine promotes the production of transforming growth factor, transforming growth factor beta (TGF-β) [8], tacrolimus reduces the TGF-β type I receptor expression on peripheral blood cells, followed by the inhibition of intracellular signal associated with TGF-β [9]. Moreover, the conversion from cyclosporine to tacrolimus induces the down-regulation of MCP-1 production in BALF [10], which has been elucidated to be one of the key chemokines in the pathogenesis of lung fibrosis [11]. These molecular mechanisms of tacrolimus may thus have led to the resolution of interstitial pneumonia in this case.

Although no cases with progressive interstitial pneumonia associated with ADM treated with tacrolimus were found in the literature, the drug has been used for patients with interstitial pneumonia associated with dermatomyositis (DM)/polymyositis (PM). Oddis et al. [12] treated five patients with anti-Jo-1 antibody-positive interstitial pneumonia and clinical improvement was obtained in three patients and disease stabilization was observed in another patient. Wilkes et al. [13] reported that DM/PM patients with refractory or severe interstitial pneumonia were all successfully treated with tacrolimus.

In summary, this case report suggests an alternative therapeutic option for progressive interstitial pneumonia associated with ADM refractory to cyclosporine. When interstitial pneumonia in ADM patients develops despite conventional immunosuppressive therapies including cyclosporin, a switch from cyclosporine to tacrolimus should be considered to rescue the patients. Further experience and clinical studies are therefore required to determine whether tacrolimus should be used prior to cyclosporine.

**Disclosures** None.

## References


1. Sontheimer RD (2009) Would a new name hasten the acceptance of amyopathic dermatomyositis (dermatomyositis sine myositis) as a distinctive subset within the idiopathic inflammatory dermatomyopathies spectrum of clinical illness? J Am Acad Dermatol 46:626–636
2. Sontheimer RD, Miyagawa S (2003) Potentially fatal interstitial lung disease can occur in clinically amyopathic dermatomyositis. J Am Acad Dermatol 48:797–798
3. Miyazaki E, Ando M, Muramatsu T, Fukami T, Matsuno O, Nureki S, Ueno T, Tsuda T, Kumamoto T (2007) Early assessment of rapidly progressive interstitial pneumonia associated with amyopathic dermatomyositis. Clin Rheumatol 26:436–439
4. Shimojima Y, Ishii W, Kato T, Hoshi K, Matsuda M, Hashimoto T, Tanaka Y, Ikeda S (2003) Intractable skin necrosis and interstitial pneumonia in amyopathic dermatomyositis, successfully treated with cyclosporin A. Intern Med 42:1253–1258
5. Suda T, Fujisawa T, Enomoto N, Nakamura Y, Inui N, Naito T, Hashimoto D, Sato J, Toyoshima M, Hashizume H, Chida K (2006) Interstitial lung diseases associated with amyopathic dermatomyositis. Eur Respir J 28:1005–1012
6. Ideura G, Hanaoka M, Koizumi T, Fujimoto K, Shimojima Y, Ishii W, Matsuda M, Ikeda S (2007) Interstitial lung disease associated with amyopathic dermatomyositis: review of 18 cases. Respir Med 101:1406–1411
7. Siekierka JJ, Hung SH, Poe M, Lin CS, Sigal NH (1989) A cytosolic binding protein for the immunosuppressant FK506 has peptidyl-prolyl isomerase activity but is distinct from cyclophilin. Nature 341:755–757
8. Shihab FS, Andoh TF, Tanner AM, Noble NA, Border WA, Franceschini N, Bennett WM (1996) Role of transforming growth factor-beta 1 in experimental chronic cyclosporine nephropathy. Kidney Int 49:1141–1151
9. Baan CC, van Riemsdijk-van Overbeeke IC, Balk AH, Vantrimpont PM, Mol WM, Knoop CJ, Niesters HG, Maat LP, Weimar W (2001) Conversion from cyclosporin A to tacrolimus is safe and decreases blood pressure, cholesterol levels and TGF-beta 1 type I receptor expression. Clin Transplant 15:276–283
10. Meloni F, Cascina A, Paschetto E, Marone Bianco A, Morosini M, Pellegrini C, Fietta A, Vitulo P, Pozzi E, Vigano M (2003) Monocyte chemoattractant protein-1 levels in bronchoalveolar lavage fluid of lung-transplanted patients treated with tacrolimus as rescue treatment for refractory acute rejection. Transplant Proc 35:1523–1526
11. Wynn TA (2008) Cellular and molecular mechanisms of fibrosis. J Pathol 214:199–210
12. Oddis CV, Sciurba FC, Elmagd KA, Starzl TE (1999) Tacrolimus in refractory polymyositis with interstitial lung disease. Lancet 353:1762–1763
13. Fau Wilkes Mr, Sereika SM, Fau Sereika Sm, Fertig N, Fau FN, Lucas MR, Fau Lucas Mr, Oddis CV, Oddis CV (2005) Treatment of antisynthetase-associated interstitial lung disease with tacrolimus. Arthritis heum 52(8):2439–2446

Clinical Neurology and Neurosurgery 111 (2009) 829–834

Contents lists available at ScienceDirect

Clinical Neurology and Neurosurgery

journal homepage: www.elsevier.com/locate/clineuro

# Evaluation of regional cerebral blood flow in cerebellar variant of multiple system atrophy using FineSRT

Noriyuki Kimura*, Toshihide Kumamoto, Teruaki Masuda, Yuki Nomura, Takuya Hanaoka, Yusuke Hazama, Toshio Okazaki

*Department of Internal Medicine III, Oita University, Faculty of Medicine, Idaigaoka 1-1, Hasama, Yufu, Oita 879-5593, Japan*

ARTICLE INFO

*Article history:*
Received 10 March 2009
Received in revised form 12 July 2009
Accepted 13 August 2009
Available online 6 September 2009

*Keywords:*
Late-onset cortical cerebellar ataxia
Cerebellar variant of multiple system atrophy
Brain perfusion SPECT
FineSRT

ABSTRACT

*Objectives:* In the present study, we compared the patterns of regional cerebral blood flow (rCBF) between cerebellar variant of multiple system atrophy (MSA-C) and the late-onset cortical cerebellar ataxia (LCCA) using FineSRT.

*Patients and methods:* We performed $^{99m}$Tc ethylcysteinate dimer (ECD) single-photon emission computed tomography in 11 patients with MSA-C (mean age 65.7 years), 7 patients with LCCA (mean age 62.0 years), and 12 age-matched healthy controls (mean age 64.1 years). The rCBF in the region of interest (ROI) was measured by the noninvasive Patlak plot method and calculated using FineSRT, which is a fully automated the ROI technique.

*Results:* All patients with MSA-C had various degrees of atrophy in the brainstem and middle cerebellar peduncles and 4 of 11 patients showed a clear 'hot cross bun' sign in pontine base on T2-weighted MR images. All patients with LCCA showed the various degrees of atrophy in cerebellum without brainstem. FineSRT revealed the significantly decreased rCBF in the caudate tail, fusiform, lingual, cerebellum, midbrain, and pons in MSA-C group compared with controls. Moreover, MSA-C group showed significantly decreased rCBF in the pons compared with LCCA group.

*Conclusion:* We suggest that a widespread brain involvement is present in patients with MSA-C and the decreased rCBF in the pons may support the differential diagnosis between MSA-C and LCCA.



## 1. Introduction

Multiple-system atrophy (MSA) is a sporadic progressive neurodegenerative disorder clinically characterized by various combinations of parkinsonian, cerebellar, autonomic, and pyramidal symptoms or signs [1,2]. MSA comprises two clinical phenotypes, such as a cerebellar variant (MSA-C) and a parkinsonian variant (MSA-P) and patients with predominantly cerebellar features are diagnosed as MSA-C. In contrast, late-onset cortical cerebellar ataxia (LCCA) is clinically characterized by a slowly progressive pure cerebellar syndrome [3,4]. The distinction MSA-C from LCCA is important for providing appropriate advice and management in the earlier stages of the disease, because MSA-C has more progressive clinical course and a poorer prognosis in comparison with LCCA [1,2]. The substantial atrophy of cerebellum, middle cerebellar peduncles, and brainstem with the 'hot cross bun' sign in the pontine base, which reflects severe degeneration of the transverse pontine fibers, are characteristic magnetic resonance imaging (MRI) findings in patients with MSA-C [5,6]. Although these MRI findings are helpful for differentiating MSA-C from LCCA, they often occur only later in the disease progression [1,2]. Single-photon emission computed tomography (SPECT) and statistical analysis techniques of SPECT images, such as three-dimensional stereotactic parametric mapping (3D-SSP), easy Z-score imaging system (eZIS), statistical parametric mapping (SPM), is sometime used to diagnose various neurodegenerative disorders [7–9]. These techniques have increased the sensitivity and accuracy of the diagnosis compared with simple visual interpretation. The objective measurement of regional cerebral blood flow (rCBF) is also essential to evaluate strictly the degree of rCBF change in the region of interest (ROI). Although the quantitative measurement of rCBF has been performed by manual settings to determine the ROI, both the reproducibility and objectivity of the results are problematic because the ROIs on the SPECT referential slice must be set equally for every patient. Takeuchi et al. developed a fully automated ROI technique such as 3DSRT and FineSRT, which allows objective assessment of rCBF in each ROI [10,11]. The aim of the present study was to objectively determine whether there was a distinguishable pattern of SPECT findings between MSA-C and LCCA using FineSRT.

* Corresponding author. Tel.: +81 97 586 5814; fax: +81 97 586 6502.
*E-mail address:* noriyuki@med.oita-u.ac.jp (N. Kimura).

0303-8467/$ – see front matter © 2009 Elsevier B.V. All rights reserved.
doi:10.1016/j.clineuro.2009.08.014

## 2. Patients and methods

### 2.1. Patients

Patients with LCCA and MSA-C admitted to the Department of Internal Medicine III, the Oita University from January 2006 to January 2009 were included in the study. The subjects were 11 patients with MSA-C (8 men and 3 women; age range 56–79 years; mean age 65.7) and 7 patients with LCCA (5 men and 2 women; age range 54–72 years; mean age 62.0). A diagnosis of MSA-C was made according to the consensus criteria proposed for probable and possible MSA [12]. Because there are no standardized criteria for diagnosing sporadic LCCA, a diagnosis of LCCA was made according to the following criteria in our study. (1) Age onset of < 30 years old; (2) pure cerebellar syndrome; (3) absence of severe abnormalities on nerve conduction studies; (4) no abnormalities on cystometry, a head-up tilt test and coefficient of variation of R-R interval; (5) no family history for an ataxia syndrome; (6) absence of a potential toxic cause that could explain the ataxia (alcoholism and anticonvulsant drugs); (7) slowly progressive disease course; (8) exclusion of cerebellar syndromes due to other causes, such as autoimmune-mediated cerebellar ataxia, paraneoplastic ataxia, alcoholic ataxia, and ataxia with hypothyroidism. Twelve similarly aged healthy control subjects (7 men and 5 women; age range 47–72 years; mean age 64.1) did not have any neurologic disorders. Informed consent was obtained from all subjects or their closest relative. All patients received a neurologic examination and their clinical evaluation was recorded using the International Cooperative Ataxia Rating Scale (ICARS) [13]. The cognitive function was evaluated using Mini-Mental State Examination (MMSE). The diagnostic evaluation included routine laboratory tests measuring the complete blood count, urine components, blood biochemistry, thyroid function, vitamin E levels, and tumor markers. For radiologic examination, brain MRI and SPECT were performed in all patients. MRI was performed using a 1.5 T scanner. The spin-echo acquisition parameters were 500–650/10–15 (TR/TE) ms for the T1-weighted axial images and 3000–4500/90 (TR/TE) for the T2-weighted axial images. The slice thickness was 5 mm with a 2.5-mm interval between successive slices. The appearance of the abnormal signal intensity in pontine base was assessed on T2-weighted images.

### 2.2. Brain SPECT imaging

Patients were asked to maintain a comfortable supine position with eyes closed in quiet surroundings. After an injection of $^{99m}$Tc ethylcysteinate dimer (600 MBq, FUJIFILM RI Pharma Co., Ltd., presently in Japan), its passage from the heart to the brain was monitored using a rectangular large field gamma camera (E. Cam Signature, Toshiba Medical, Japan). For the quantification of regional CBF (rCBF), the Patlak plot method [14,15] was employed on $^{99m}$Tc ethylcysteinate dimer cerebral blood perfusion SPECT to measure mean cerebral blood flow (mCBF). Quantitative flow-mapping images were obtained from the qualitative cerebral perfusion SPECT images by using Patlak plot graphical analysis and Lassen's correction [14–16]. Data acquisition was a sequence of 120 frames at a rate of 1 s per frame with a 128 × 128 matrix. Ten minutes after the angiography, SPECT images were obtained using a rotating, dual-head gamma camera (E. Cam Signature) equipped with low energy, high resolution and parallel hole collimators. The energy windows were set at 140 keV ± 20% and 90 views were obtained throughout 360° of rotation (128 × 128 matrix, 1.95 mm/pixel) with an acquisition time of 140 s/cycle repeated 6 times. Data processing was performed on a GMS-7700A/EI (Toshiba Medical, Japan). All images were reconstructed using ramp-filtered backprojection and then three-dimensionally smoothed with a Butterworth filter (order 8, cutoff 0.25 cycles/pixcel). The reconstructed images were corrected for gamma ray attenuation using the Chang method ($\mu = 0.09$).

**Table 1**
Summary of the clinical and demographic characteristics for LCCA and MSA-C groups. LCCA: late-onset cortical cerebellar ataxia. MSA-C: cerebellar variant of multiple system atrophy. mCBF: mean value of the cerebral blood flow in the bilateral cerebral hemisphere.

| | MSA-C ($n = 11$) | LCCA ($n = 7$) | Control subjects ($n = 12$) |
|---|---|---|---|
| Sex (male/female) | 8/3 | 5/2 | 7/5 |
| Age (year) | 65.7 ± 7.6 | 62.0 ± 7.7 | 64.1 ± 8.6 |
| Disease duration (year) | 3.3 ± 1.6 | 5.4 ± 4.4 | |
| ICARS | 40.0 ± 21.6 | 30.7 ± 14.1 | |
| mCBF (ml/100 g/min) | 40.2 ± 3.7 | 40.8 ± 3.5 | 41.6 ± 4.2 |

### 2.3. SPECT image analysis using FineSRT

Quantitative flow-mapping images were obtained from the qualitative perfusion images using Patlak plot graphical analysis and Lassen's correction, as previously reported [14–16]. The rCBF in each regions of interest (ROI) was calculated using software named FineSRT, which is a fully automated ROI technique developed by Takeuchi et al. [10]. FineSRT performed by consecutive analyzing process as follows: (1) anatomical standardization using the SPM99 algorithm; (2) analysis using constant 812 ROIs divided into 10 groups (segments) on each hemisphere; (3) calculation of the area-weighted average for each of the respective 52 segments; (4) display of the results followed by the saving of respective values of the 1624 ROIs (both hemispheres). These ROIs were categorized into 52 subsegments; superior frontal, medial frontal, paracentral lobule, anterior cingulate, subcallosal, orbital, rectal, middle frontal, inferior frontal, precentral, postcentral, insula, superior parietal, inferior parietal, supramarginal, angular, superior temporal, middle temporal, inferior temporal, transverse temporal, superior occipital, middle occipital, inferior occipital, precuneus, lower cuneus, hippocampus, fusiform, lingual, parahippocampal, amygdaloid body, thalamus, putamen, globus pallidus, caudate head, caudate tail, precuneus upper, cingulate, posterior cingulate, vermis, anterior lobe of cerebellum, posterior lobe of cerebellum, quadrigemini, substantia nigra, nucleus ruber, pons, Broca, Wernicke, primary visual, primary auditory, premotor, supplementary motor segments in the template. Moreover, we lumped together the midbrain structures such as quadrigemina, substantia nigra, and red nucleus, and described them as midbrain ROI, because each structure of midbrain is too small to be evaluated strictly. The rCBF is expressed as the mean value ± standard deviation for each bilateral segment.

### 2.4. Statistical analysis

The differences in the rCBF of all 50 subsegments were analyzed using the Mann–Whitney $U$ test. A $p$ value of less than 0.01 was considered to be statistically significant.

## 3. Results

Table 1 summarizes the clinical and demographic characteristics of the patients with LCCA and MSA-C and control subjects. The groups did not differ significantly in terms of age and sex. The mean disease duration in LCCA group (5.4 ± 4.4 years) was longer than that in MSA-C group (3.3 ± 1.6 years), but this was not statistically significant. On neurologic examination, patients with MSA-C revealed limb ataxia, truncal ataxia and ataxic gait with parkinsonism, autonomic, and pyramidal signs, whereas patients with LCCA

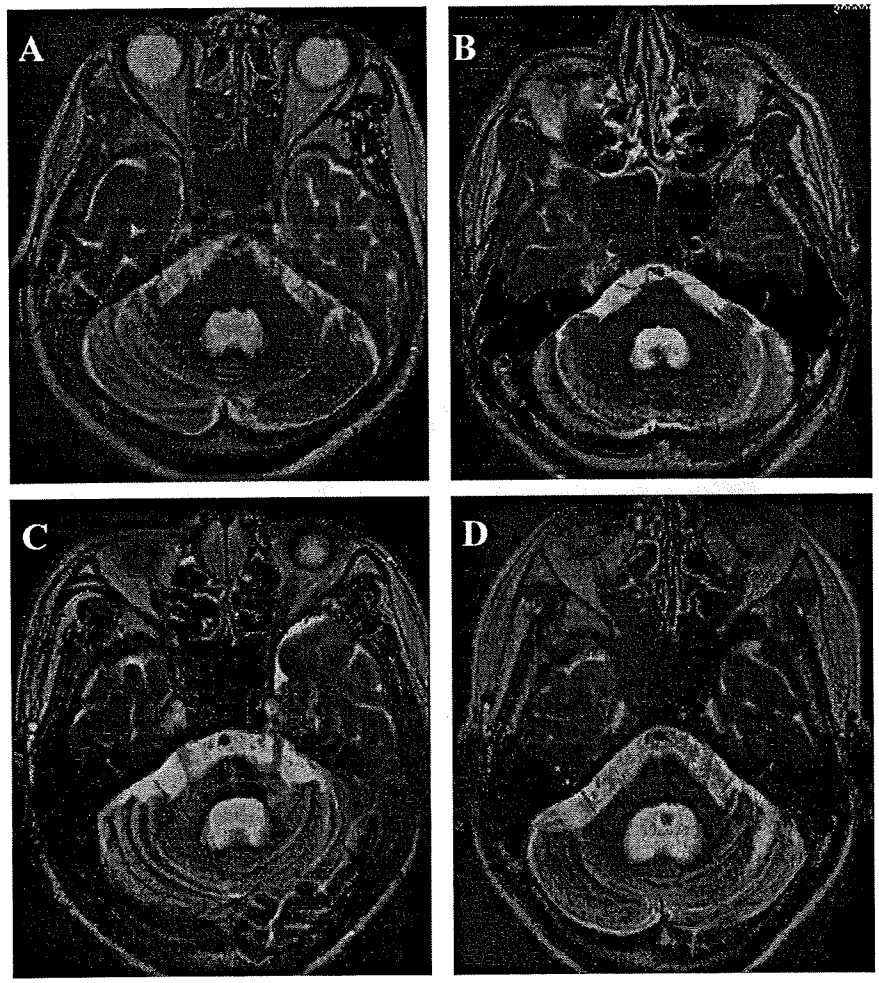


**Fig. 1.** T2-weighted MR images (axial images) in patients with MSA-C (A–D). The degree of brain atrophy in the cerebellum, pons, and middle cerebellar peduncles was various as follow; mild to moderate (A and B) and severe (C and D). Abnormal signal hyperintensity in the pontine base was clearly observed (C).

showed limb ataxia, truncal ataxia, ataxic gait, and/or gaze-evoked nystagmus. The mean ICARS value in MSA-C group ($40.0 \pm 21.6$) was higher than that in LCCA group ($30.7 \pm 14.2$), which was not a statistically significant. All patients with MSA-C and LCCA did not have significant cognitive impairment. The mean MMSE values were $29.4 \pm 1.8$ (range, 24–30) in MSA-C group and $29.1 \pm 2.3$ (range, 24–30) in LCCA group. The mean whole brain CBF value did not differ significantly between the patients with MSA-C and LCCA and control subjects. MRI demonstrated various degrees of atrophy in the cerebellar hemisphere, vermis, middle cerebellar peduncles, and brainstem in all patients with MSA-C (Fig. 1). Moreover, abnormal signal hyperintensity in the pontine base and middle cerebellar peduncles, which is characteristic of MSA, was clearly observed in 4 of 11 patients on T2-weighted MR images. All the patients with LCCA showed various degrees of atrophy in the cerebellar vermis and hemisphere without the brainstem atrophy or abnormal signal hyperintensity. The visual analysis of SPECT images could detect the significantly decreased rCBF in medial temporal lobe and cerebellum in patients with LCCA and in medial temporal lobe basal ganglia, cerebellum, and brainstem in patients with MSA-C. However, it was difficult to identify the slightly decreased rCBF by the visual analysis of SPECT images (Fig. 2). A group comparison of rCBF values in each ROI using FineSRT between LCCA, MSA-C, and controls is shown in Table 2. The MSA-C group had significantly lower rCBF values in the fusiform, lingual, caudate tail, vermis, anterior and posterior cerebellar lobes, midbrain and pons than did controls (fusiform, $p = 0.0002$; lingual, $p = 0.0026$; caudate tail, $p = 0.0031$; vermis; $p < 0.0001$, anterior cerebellar lobe, $p < 0.0001$; posterior cerebellar lobe, $p < 0.0001$; midbrain, $p = 0.0071$; pons, $p < 0.0001$). The LCCA group had significantly lower rCBF values in the fusiform, vermis, anterior and posterior cerebellar lobes than in did controls (fusiform, $p = 0.0013$; vermis, $p = 0.0018$; anterior cerebellar lobe, $p = 0.0007$; posterior cerebellar lobe, $p = 0.0031$). Moreover, rCBF in the pons was significantly lower in the MSA-C group than in the LCCA group (pons, $p = 0.0007$) (Fig. 3). In particular, the rCBF values in pons were lower in 10 of 11 patients with MCA-C compared with the patients with LCCA. The cerebellar rCBF in the MSA-C group were relatively lower than that in the LCCA group, but the difference was not significant. The rCBF was relatively lower in putamen, globus pallidus, and caudate head in patients with MSA-C compared with the patients with LCCA and controls, but this was not significant.

## 4. Discussion

In present study, we performed the quantitative analysis of rCBF using FineSRT to precisely detect abnormal rCBF pattern in the patients with MSA-C and LCCA. The FineSRT analysis revealed that the rCBF values were significantly lower in the caudate tail, fusiform, lingual, cerebellum, and brainstem such as pons and

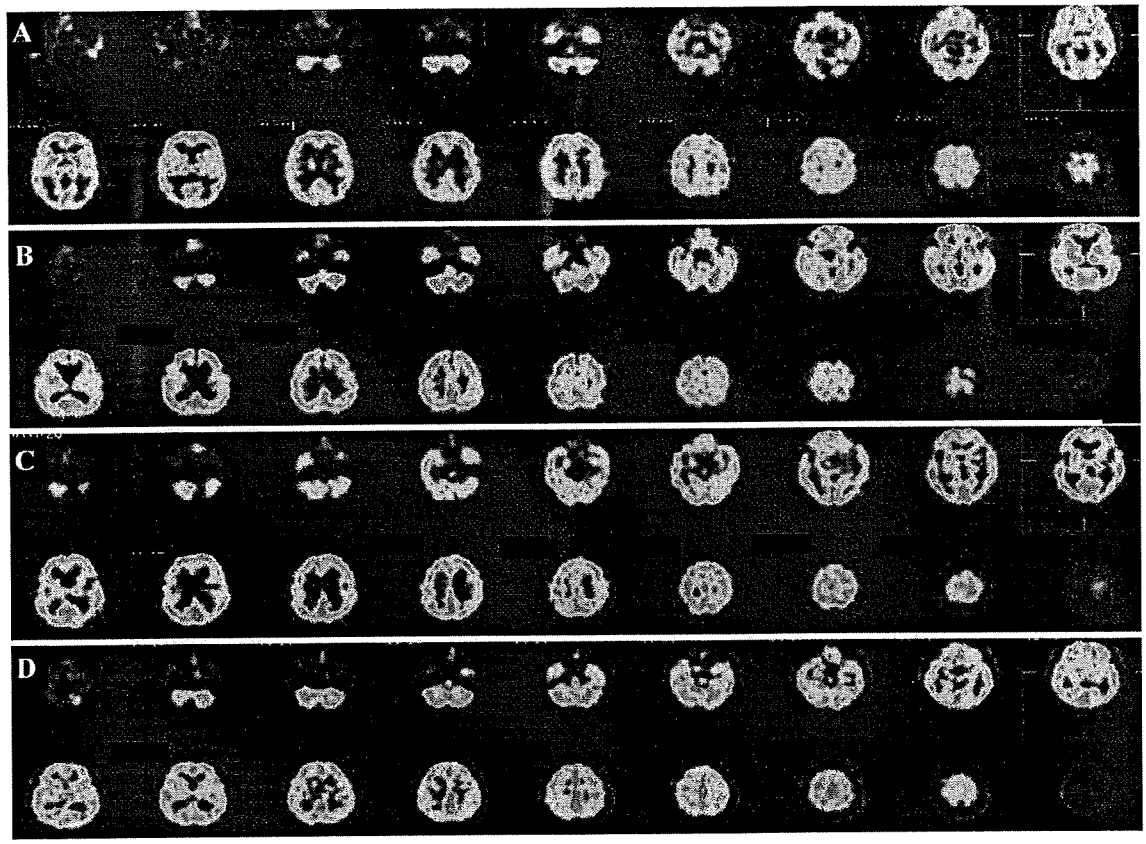


**Fig. 2.** SPECT images (axial view) in patients with LCCA and MSA-C. The significantly decreased rCBF could be detected obviously in medial temporal lobe and cerebellum in patients with LCCA (A), and in medial temporal lobe basal ganglia, cerebellum, and brainstem in patients with MSA-C (C). It is difficult to detect the slightly decreased rCBF by the visual analysis in some patients with LCCA (C) and MSA-C (D). LCCA: late-onset cortical cerebellar ataxia. MSA-C: cerebellar variant of multiple system atrophy.

**Table 2**
Regional cerebral blood flow (rCBF) in each ROI compared between the LCCA, MSA-C, and control groups. LCCA: late-onset cortical cerebellar ataxia. MSA-C: cerebellar variant of multiple system atrophy. rCBF: regional cerebral blood flow. $^{*}p < 0.01$ compared to controls. $^{**}p < 0.01$ compared to control and LCCA groups.

| Region | rCBF(ml/100 g/min) | | | Region | rCBF(ml/100 g/min) | | |
|---|---|---|---|---|---|---|---|
| | MSA-C | LCCA | Control | | MSA-C | LCCA | Control |
| Superior frontal | 40.0 ± 4.3 | 39.3 ± 4.7 | 39.0 ± 4.0 | Hippocampus | 27.6 ± 3.5 | 30.5 ± 3.8 | 31.3 ± 4.2 |
| Medial frontal | 42.4 ± 4.6 | 41.8 ± 5.3 | 41.8 ± 5.1 | Fusiform | 32.9 ± 2.3* | 33.5 ± 2.4* | 39.8 ± 4.2 |
| Paracentral lobule | 44.3 ± 7.0 | 44.3 ± 5.8 | 44.9 ± 7.9 | Lingual | 37.5 ± 2.6* | 37.5 ± 4.1 | 43.7 ± 4.6 |
| Anterior cingulate | 32.8 ± 5.1 | 36.1 ± 5.1 | 33.7 ± 4.3 | Parahippocampal | 30.5 ± 2.3 | 31.8 ± 2.6 | 33.1 ± 3.6 |
| Subcallosal | 37.9 ± 5.4 | 42.9 ± 3.7 | 39.5 ± 5.2 | Amygdaloid body | 26.1 ± 4.9 | 27.8 ± 2.7 | 28.0 ± 3.8 |
| Orbital | 37.5 ± 4.5 | 40.6 ± 3.4 | 39.6 ± 3.5 | Thalamus | 37.4 ± 6.0 | 42.0 ± 5.3 | 41.9 ± 6.3 |
| Rectal | 36.3 ± 4.9 | 38.4 ± 4.2 | 37.7 ± 3.7 | Putamen | 41.8 ± 4.8 | 45.5 ± 2.7 | 45.4 ± 5.6 |
| Middle frontal | 42.0 ± 3.8 | 42.2 ± 5.0 | 41.9 ± 4.2 | Globus pallidus | 36.4 ± 5.3 | 39.4 ± 2.7 | 41.1 ± 5.6 |
| Inferior frontal | 38.5 ± 4.5 | 39.6 ± 4.0 | 39.3 ± 3.4 | Caudate head | 26.6 ± 6.7 | 29.8 ± 5.6 | 29.6 ± 5.6 |
| Precentral | 38.9 ± 4.0 | 37.3 ± 5.4 | 39.6 ± 3.8 | Caudate tail | 20.9 ± 3.7* | 24.0 ± 3.2 | 25.6 ± 2.9 |
| Postcentral | 37.0 ± 3.3 | 37.0 ± 4.4 | 38.4 ± 4.1 | Precuneus upper | 40.6 ± 4.9 | 41.2 ± 4.7 | 42.8 ± 5.7 |
| Insula | 35.8 ± 4.7 | 40.5 ± 2.2 | 39.3 ± 3.9 | Cingulate | 35.2 ± 3.5 | 37.0 ± 4.0 | 38.1 ± 3.9 |
| Superior parietal | 34.7 ± 2.7 | 34.7 ± 3.8 | 36.5 ± 4.4 | Posterior cingulate | 41.9 ± 3.4 | 42.8 ± 3.9 | 44.3 ± 5.8 |
| Inferior parietal | 37.6 ± 3.2 | 37.3 ± 4.3 | 39.1 ± 3.7 | Vermis | 31.3 ± 4.7* | 35.8 ± 6.3* | 48.6 ± 5.9 |
| Supramarginal | 37.4 ± 3.1 | 37.4 ± 3.5 | 39.9 ± 3.7 | Anterior lobe (cerebellum) | 29.2 ± 2.7* | 30.7 ± 3.5* | 41.6 ± 4.0 |
| Angular | 39.0 ± 2.9 | 38.3 ± 3.8 | 41.7 ± 4.4 | Posterior lobe (cerebellum) | 36.9 ± 5.0* | 41.0 ± 6.4* | 51.7 ± 4.7 |
| Superior temporal | 34.6 ± 3.9 | 34.9 ± 2.9 | 36.9 ± 3.6 | Midbrain | 25.2 ± 4.8 | 31.9 ± 4.6 | 33.2 ± 4.6 |
| Middle temporal | 35.6 ± 2.7 | 35.4 ± 3.4 | 37.2 ± 3.5 | Pons | 19.2 ± 3.2** | 29.7 ± 4.7 | 30.9 ± 4.2 |
| Inferior temporal | 34.4 ± 2.8 | 34.2 ± 3.4 | 35.4 ± 3.0 | Broca | 38.0 ± 4.6 | 38.9 ± 4.5 | 38.7 ± 3.9 |
| Transverse temporal | 37.0 ± 5.6 | 40.6 ± 4.7 | 41.1 ± 6.1 | Wernicke | 39.4 ± 3.7 | 38.6 ± 3.0 | 42.2 ± 4.0 |
| Superior occipital | 34.2 ± 2.7 | 34.4 ± 4.6 | 37.1 ± 3.6 | Primary visual | 40.8 ± 3.0 | 39.0 ± 5.2 | 43.0 ± 4.4 |
| Middle occipital | 34.4 ± 3.2 | 34.3 ± 3.2 | 37.2 ± 3.2 | Primary auditory | 36.6 ± 5.2 | 39.4 ± 4.2 | 40.1 ± 5.0 |
| Inferior occipital | 32.9 ± 2.8 | 33.0 ± 2.3 | 36.2 ± 3.4 | Premotor | 38.8 ± 4.2 | 38.0 ± 4.2 | 38.8 ± 3.9 |
| Precuneus lower | 45.6 ± 3.2 | 47.1 ± 5.4 | 49.0 ± 6.8 | Supplementary motor | 42.5 ± 6.8 | 40.1 ± 5.1 | 42.9 ± 6.8 |
| Cuneus | 41.6 ± 2.6 | 40.5 ± 4.8 | 44.4 ± 3.7 | | | | |

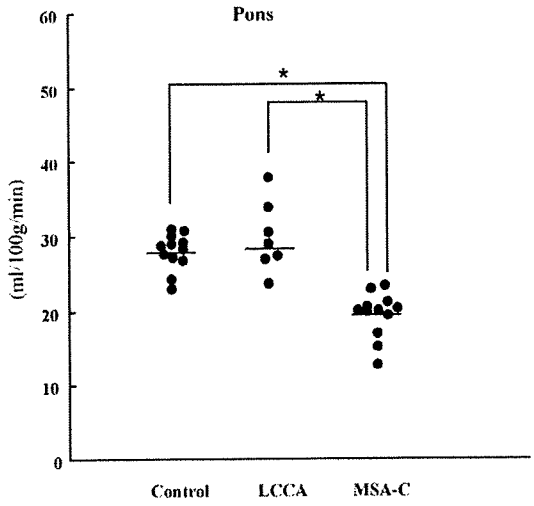


Fig. 3. Regional cerebral blood flow (rCBF) in the pons compared between the LCCA, MSA-C, and control groups. The rCBF was significantly decreased in the pons in MSA-C group compared with LCCA group and controls. The rCBF values in pons were lower in 10 of 11 patients with MCA-C compared with the patients with LCCA. *$p < 0.01$. LCCA: late-onset cortical cerebellar ataxia. MSA-C: cerebellar variant of multiple system atrophy.

midbrain in MSA-C group compared with controls. The relatively decreased rCBF in the cerebellum, pons, and/or midbrain was reported in the patients with MSA-C using eZIS and SPM analysis [8,17], but it has also been reported that a remarkable rCBF reduction in the brainstem could not be identified using SPM analysis [9,18]. The eZIS and SPM2 results demonstrated a Z-score map for each SPECT image, which was extracted from the comparison with the mean and SD of SPECT images of controls and enabled us to objectively detect cerebral regions with relatively decreased blood perfusion [7–9]. Whereas the FineSRT program allows for the objective assessment of rCBF value by automatically setting the ROIs based on standardized SPECT images [10,11]. Our results of FineSRT analysis were consistent with the previously reported SPECT patterns, which showed decreased rCBF in the brainstem in the patients with MSA-C. The rCBF in basal ganglia was relatively lower in MSA-C group compared with controls, but the significant hypoperfusion was limited to the caudate tail. These findings correspond with the neuropathological findings of MSA-C because MSA-C show the less degeneration of basal ganglia, including putamen, caudate nucleus and globus pallidus compared with MSA-P [19]. Moreover, the significantly decreased rCBF value was also observed in the medial temporal lobe, such as fusiform and/or lingual in the MSA-C as well as LCCA groups. Previous studies reported that patients with MSA and LCCA presented the cognitive dysfunction and cortical involvement [18,20–22]. MSA-C showed a various degree of widespread cerebral atrophy, particularly in the frontal and temporal lobe, in the studies based on longitudinal voxel-based morphometry [23] and LCCA revealed a frontal lobe hypoactivities in the analysis of electroencephalography and mid-latency auditory evoked responses [24]. Although our patients with MSA-C and LCCA had normal cognitive function, one possible explanation for the hypoperfusion in fusiform and lingual might be a primary disease process or degeneration of cerebellocortical projections affected the cerebral cortex.

In the present study, we compared a disease-specific abnormal rCBF pattern in MSA-C to that in LCCA. At the earlier stages of the disease, it is difficult to distinguish MSA-C from LCCA because MSA-C initially develops cerebellar symptoms followed by noncerebellar symptoms such as parkinsonian, cerebellar, autonomic dysfunction, and pyramidal signs. Although characteristic MR images including the 'hot cross bun' sign in the pontine base may be useful for making a correct diagnosis of MSA-C, the frequency of signal abnormalities in the pontine base is only 47.8% in patients with MSA-C within 4 years from the time of onset [1,2]. All of our patients with MSA-C demonstrated various degrees of atrophy in the brainstem and middle cerebellar peduncle, however only 4 of 11 patients had a clear 'hot cross bun' sign in pontine base because the mean disease duration was less than 4 years. The FineSRT analysis results showed that MSA-C group had significantly decreased rCBF in the pons compared with LCCA group, despite the lack of significant difference of mean value of CBF in the whole brain as well as other brain regions. In particular, the rCBF values in pons were lower in 10 of 11 patients with MCA-C compared to the LCCA group, regardless of the disease duration and the appearance of 'hot cross bun' sign on MRI. Therefore, we suggest that the decreased rCBF in the pons combined with the MRI findings may support the differential diagnosis between MSA-C and LCCA. Although the cerebellar rCBF was lower in MSA-C group than in LCCA group, these findings cannot support the differential diagnosis between MSA-C and LCCA. These rCBF patterns may reflect the different distributions and severity of neuronal degeneration between MSA-C and LCCA, because the widespread and severe brain involvement, including striatonigral region, olivopontocerebellar region, and autonomic nervous system is present in MSA-C [1,2,25], whereas the pathologic changes are mainly limited to the cerebellar cortex and inferior olivary nucleus in LCCA [26].

There are several limitations to the present study. The number of patients with MSA-C and LCCA was relatively small and further studies with bigger samples, including are needed to confirm our results.

## 5. Conclusion

The FineSRT findings indicate that more widespread brain involvement is present in patients with MSA-C at earlier stage. We suggest that the decreased rCBF in the pons may support the differential diagnosis between MSA-C and LCCA.

## References

[1] Yabe I, Soma H, Takei A, Fujiki N, Yanagihara T, Sasaki H. MSA-C is the predominant clinical phenotype of MSA in Japan: analysis of 142 patients with probable MSA. J Neurol Sci 2006;249:115–21.
[2] Watanabe H, Saito Y, Terao S, Ando T, Kachi T, Mukai E, et al. Progression and prognosis in multiple system atrophy: an analysis of 230 Japanese patients. Brain 2002;125:1070–83.
[3] Tsuchiya K, Ozawa E, Saito F, Irie H, Mizutani T. Neuropathology of late cortical cerebellar atrophy in Japan: distribution of cerebellar change on an autopsy case and review of Japanese cases. Eur Neurol 1994;34:253–62.
[4] Hirayama K, Takayanagi T, Nakamura R, Yanagisawa N, Hattori T, Kita K, et al. Spinocerebellar degenerations in Japan: a nationwide epidemiological and clinical study. Acta Neurol Scand 1994;153:1–22.
[5] Savoiardo M, Strada L, Girotti F, Zimmerman RA, Grisoli M, Testa D, et al. Olivopontocerebellar atrophy: MR diagnosis and relationship to multisystem atrophy. Radiology 1990;174:693–6.
[6] Adachi M, Hosoya T, Yamaguchi K, Kawanami T, Kato T. Diffusion- and T2-weighted MRI of the transverse pontine fibres in spinocerebellar degeneration. Neuroradiology 2000;42:803–9.
[7] Kuwabara Y. Advance of SPECT: differential diagnosis and evaluation of pathophysiology of neurodegenerative disorders. Rinsho Shinkeigaku 2004;44:894–6.
[8] Waragai M, Yamada T, Matsuda H. Evaluation of brain perfusion SPECT using an easy Z-score imaging system (eZIS) as an adjunct to early-diagnosis of neurodegenerative diseases. J Neurol Sci 2007;260:57–64.
[9] Watanabe H, Sugihara H, Horiuchi M, Takahashi Y. Analysis of brain images in patients with spinocerebellar degeneration, using statistical parametric mapping (SPM) and easy Z score imaging system (eZIS). Kaku Igaku 2005;42:107–13.
[10] Takeuchi R, Sengoku T, Matsumura K. Usefulness of fully automated constant ROI analysis software for the brain: 3DSRT and FineSRT. Radiat Med 2006;24:538–44.

[11] Tateno M, Kobayashi S, Utsumi K, Morii H, Fujii K. Quantitative analysis of the effects of donepezil on regional cerebral blood flow in Alzheimer's disease by using an automated program, 3DSRT. Neuroradiology 2008;50:723–7.
[12] Gilman S, Low PA, Quinn N, Albanese A, Ben-Shlomo Y, Fowler CJ, et al. Consensus statement on the diagnosis of multiple system atrophy. J Neurol Sci 1999;163:94–8.
[13] Trouillas P, Takayanagi T, Hallett M, Currier RD, Subramony SH, Wessel K, et al. International cooperative ataxia rating scale for pharmacological assessment of the cerebellar syndrome. The Ataxia Neuropharmacology Committee of the World Federation of Neurology. J Neurol Sci 1997;145:205–11.
[14] Friberg L, Andersen AR, Lassen NA, Holm S, Dam M. Retention of 99mTc-bicisate in the human brain after intracarotid injection. J Cereb Blood Flow Metab 1994;14:19–27.
[15] Matsuda H, Tsuji S, Shuke N, Sumiya H, Tonami N, Hisada K. Noninvasive measurements of regional cerebral blood flow using technetium-99m hexamethylpropylene amine oxime. Eur J Nucl Med 1993;20:391–401.
[16] Lassen NA, Andersen AR, Friberg L, Paulson OB. The retention of [99mTc]-d,l-HM-PAO in the human brain after intracarotid bolus injection: a kinetic analysis. J Cereb Blood Flow Metab 1988;8:13–22.
[17] Cilia R, Marotta G, Benti R, Pezzoli G, Antonini A. Brain SPECT imaging in multiple system atrophy. J Neural Transm 2005;112:1635–45.
[18] Kawai Y, Suenaga M, Takeda A, Ito M, Watanabe H, Tanaka F, et al. Cognitive impairments in multiple system atrophy: MSA-C vs MSA-P. Neurology 2008;15(70):1390–6.
[19] Jellinger KA, Seppi K, Wenning GK. Grading of neuropathology in multiple system atrophy: proposal for a novel scale. Mov Disord 2005;20:S29–36.
[20] Konagaya M, Konagaya Y, Sakai M, Matsuoka Y, Hashizume Y. Progressive cerebral atrophy in multiple system atrophy. J Neurol Sci 2002;195:123–7.
[21] Suenaga M, Kawai Y, Watanabe H, Atsuta N, Ito M, Tanaka F, et al. Cognitive impairment in spinocerebellar ataxia type 6. J Neurol Neurosurg Psychiatry 2008;79:496–9.
[22] Liszewski CM, O'Hearn E, Leroi I, Gourley L, Ross CA, Margolis RL. Cognitive impairment and psychiatric symptoms in 133 patients with diseases associated with cerebellar degeneration. J Neuropsychiatry Clin Neurosci 2004;16:109–12.
[23] Brenneis C, Boesch SM, Egger KE, Seppi K, Scherfler C, Schocke M, et al. Cortical atrophy in the cerebellar variant of multiple system atrophy: a voxel-based morphometry study. Mov Disord 2006;21:159–65.
[24] Arai M, Tanaka H, Pascual-Marqui RD, Hirata K. Reduced brain electric activities of frontal lobe in cortical cerebellar atrophy. Clin Neurophysiol 2003;114:740–7.
[25] Ozawa T, Paviour D, Quinn NP, Josephs KA, Sangha H, Kilford L, et al. The spectrum of pathological involvement of the striatonigral and olivopontocerebellar systems in multiple system atrophy: clinicopathological correlations. Brain 2004;127:2657–71.
[26] Ota S, Tsuchiya K, Anno M, Niizato K, Akiyama H. Distribution of cerebello-olivary degeneration in idiopathic late cortical cerebellar atrophy: clinicopathological study of four autopsy cases. Neuropathology 2008;28:43–50.

Journal of the Neurological Sciences 287 (2009) 281–284

Contents lists available at ScienceDirect

Journal of the Neurological Sciences

journal homepage: www.elsevier.com/locate/jns

Short communication

# Primary central nervous system lymphoma with cortical laminar hemorrhage

Noriyuki Kimura [a,*], Masato Ishibashi [a], Teruaki Masuda [a], Masaki Morishige [b], Tatsuya Abe [b], Minoru Fujiki [b], Kenji Kashima [c], Toshihide Kumamoto [a]

[a] Department of Internal Medicine III, Oita University, Faculty of Medicine, Oita, Japan
[b] Department of Neurosurgery, Oita University, Faculty of Medicine, Oita, Japan
[c] Pathology Center, Oita University Hospital, Faculty of Medicine, Oita, Japan

ARTICLE INFO

*Article history:*
Received 7 March 2009
Received in revised form 17 July 2009
Accepted 24 July 2009
Available online 21 August 2009

*Keywords:*
Primary central nervous system lymphoma
Cortical laminar hemorrhage
Brain biopsy
Vascular endothelial growth factor
Magnetic resonance imaging (MRI)

ABSTRACT

Here we report a case of primary central nervous system (CNS) lymphoma with cortical laminar hemorrhage. The present case showed an acute onset of focal neurologic signs and bilateral cortical lesions surrounded by peripheral white matter edema on magnetic resonance imaging. A part of the left frontal cortical lesion was hyperintense on T1-weighted images and hypointense on T2-weighted and T2*-weighted gradient-echo images, suggesting subacute laminar hemorrhage. The patient was initially diagnosed with multiple hemorrhagic infarctions, but a biopsy specimen revealed diffuse large B-cell lymphoma with hemosiderin deposits. Immunohistochemical studies revealed that the tumor cell cytoplasm and membrane stained positively for anti-vascular endothelial growth factor antibody. The present case reconfirms the danger of making a specific lymphoma diagnosis based on magnetic resonance imaging findings alone and that histopathologic examination following brain biopsy is necessary for a correct diagnosis. Vascular endothelial growth factor expression might be associated with the intratumoral hemorrhage.



## 1. Introduction

Primary central nervous system (CNS) lymphoma is relatively rare, representing only 1% to 2% of all primary CNS malignancies [1]. The vast majority of primary CNS lymphomas are diffuse large B-cell lymphomas, regardless of the patient's immunologic state, and primary T-cell lymphomas are uncommon in the CNS [2,3]. The frequency of CNS lymphoma in both immunocompromised and immunocompetent patients has increased over the last decade, however, atypical clinical and radiologic presentations are becoming more common [4,5]. Although an early and reliable diagnosis of CNS lymphoma is important to initiate rapidly optimal therapy, such atypical cases complicate the differential diagnosis by clinicians and radiologists. The presence of hemorrhage is used to exclude primary cerebral lymphoma in the differential diagnosis, because hemorrhagic lesions are extremely rare in immunocompetent patients with primary CNS lymphoma [6–9].

We describe an immunocompetent patient who presented with multiple supratentorial lesions with cortical laminar hemorrhage. The patient was initially diagnosed with multiple hemorrhagic infarctions, but histologic examination revealed a primary CNS B-cell type lymphoma. To our knowledge, there are no reports of cortical laminar hemorrhage in an immunocompetent case of primary CNS lymphoma. Here, we discuss the radiologic and neuropathologic manifestations of this case together with a brief overview of the relevant literature.

## 2. Case report

In February 2008, a 57-year-old right-handed Japanese female developed sudden-onset mild weakness in her right upper extremity and dysarthria. Four weeks later, the patient was admitted to a local hospital with a mild consciousness disturbance and worsening of the described neurologic symptoms. Brain MRI revealed multiple lesions with a mild mass effect in the left frontal and right parietal lobes. Additionally, the cortex of the left frontal lesion contained a subacute laminar hemorrhage. Although the patient was placed on anticoagulant therapy with rehabilitation for suspected subacute hemorrhagic infarctions, the neurologic symptoms gradually worsened. She was admitted to our hospital for further evaluation at the beginning of March. On admission, she was drowsy and had a Mini-Mental State examination score of 24 points. Neurologic examination revealed mild right hemifacial palsy, mild right hemiparesis, and hyperreflexia in the right extremities without pathologic reflex. She had no known congenital or acquired immunodeficiency. Routine blood tests and cerebrospinal fluid analysis were normal. Bacterial and fungal cultures were negative and the anti-viral titer in the serum and cerebrospinal fluid was not markedly increased. Electroencephalography showed intermittent slow waves in the left frontal region. Follow-up MRI 2 months after onset revealed that the left frontal and right parietal lesions had increased in size compared to the previous MRI findings

* Corresponding author. Department of Internal Medicine III, Oita University, Faculty of Medicine, Idaigaoka 1-1, Hasama, Yufu, Oita 879-5593, Japan. Tel.: +81 97 586 5814; fax: +81 97 586 6502.
*E-mail address:* noriyuki@med.oita-u.ac.jp (N. Kimura).

0022-510X/$ – see front matter © 2009 Elsevier B.V. All rights reserved.
doi:10.1016/j.jns.2009.07.022

(Fig. 1a–f). The laminar hemorrhage in the left frontal cortex was hyperintense on T1-weighted images (Fig. 1a) and hypointense on T2-weighted (Fig. 1c) and gradient-echo T2*-weighted images (Fig. 1f). The cortex adjacent to the laminar hemorrhage in the left frontal and right parietal cortical lesions was slightly hypointense on T1-weighted images and hyperintense on T2-weighted images. Contrast-enhanced T1-weighted images showed dense focal enhancement in the cortical lesions (Fig. 1b). These lesions were surrounded by subcortical white matter edema that appeared homogeneously hypointense on T1-weighted images and hyperintense on T2-weighted images. The enhanced area in the left frontal cortex had a higher signal intensity on diffusion-weighted imaging (DWI; Fig. 1d) with lower apparent diffusion coefficient (ADC) values (Fig. 1e) than the peripheral edema (median $ADC_{\text{left cortical lesions}} = 88.8 \times 10^{-7}$ cm$^2$/s, median $ADC_{\text{perifocal edema}} = 168.2 \times 10^{-7}$ cm$^2$/s). The ADC value of the right enhanced area was too small to measure. The results of magnetic resonance angiography appeared normal. Thallium-201 brain single photon emission computed tomography ($^{201}$Tl SPECT) showed high uptake of the tracer in both lesions at the early and late phases. The initial diagnosis of subacute hemorrhagic infarctions was not compatible with the progressive course of the disease with an expanding lesion and the SPECT findings. The differential diagnosis for malignant lesions included metastatic brain tumor, multiple glioma, primary CNS lymphoma, and intravascular lymphomatosis, whereas that for benign lesions included demyelinating diseases, meningoencephalitis with vasculitis, status epilepticus, and neurosarcoidosis. Therefore, the patient was transferred to neurosurgery for a left frontal craniotomy and open biopsy on the 14th hospital day. The gross appearance of the lesion, which was easily distinguished from the adjacent normal cortex, was yellow-gray discoloration and firm. Brain biopsy specimens were obtained from the gadolinium-enhanced area and adjacent hemorrhagic areas in the left frontal cortex. The gadolinium-enhanced area appeared grayish in color macroscopically and histopathologically revealed hypercellular infiltration of malignant lymphocytes around the cerebral blood vessels (Fig. 2a), whereas the adjacent hemorrhagic area was yellowish discoloration and histopathologically showed slight infiltration of malignant lymphocytes with hemosiderin deposits (Fig. 1d). The gadolinium-enhanced area, which involved the cortex, was related to the tumor itself. Pathologic findings of intravascular lymphomatosis were not identified throughout in any of the lesions. There was no evidence of cortical laminar necrosis, such as neuronal ischemia accompanied by gliosis or a layered deposition of fat-laden macrophages [10] in the adjacent hemorrhagic area. Numerous iron-reactive granules were detected by Perls's stain with Brazilian counterstaining in the hemorrhagic area (Fig. 1e). The tumor cells

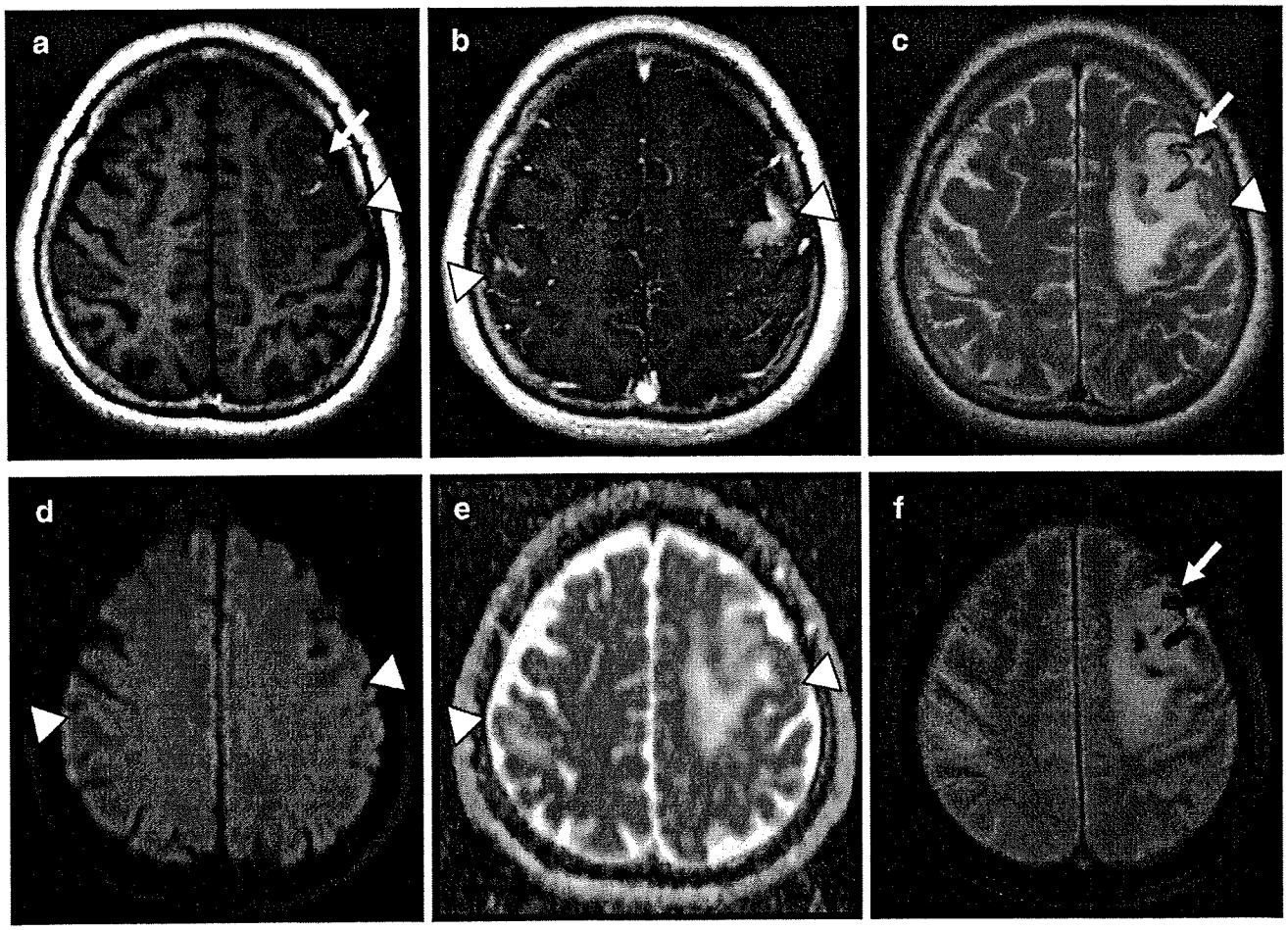


**Fig. 1.** Cranial MRI of the lesions in left frontal lobe and right postcentral gyrus. The right side is shown on the left-hand side of each figure. a. Axial T1-weighted image demonstrates a hypointense area with focal hyperintensity (arrows) in the left frontal cortex and a small hypointense area in the right postcentral cortex. These lesions were surrounded by white matter edema that appeared homogeneously hypointense on T1-weighted images. b. Axial gadolinium-enhanced T1-weighted image shows focal enhancement of the cortical lesions in both hemispheres. c. Axial T2-weighted image shows slightly hyperintense area with focal hypointensity (arrows) in the left frontal cortex, and a slightly hyperintense area of the right postcentral gyrus. These lesions were surrounded by white matter edema that appeared homogeneously hyperintense on T2-weighted images. d, e. All lesions show high signal intensity on diffusion-weighted image (DWI) and slight low ADC values, while peripheral edema is slightly hypointense on DWI with elevated ADC values. f. Axial gradient-echo T2*-weighted image demonstrated hypointensity of the cortical laminar hemorrhage in the left frontal cortex (arrows).

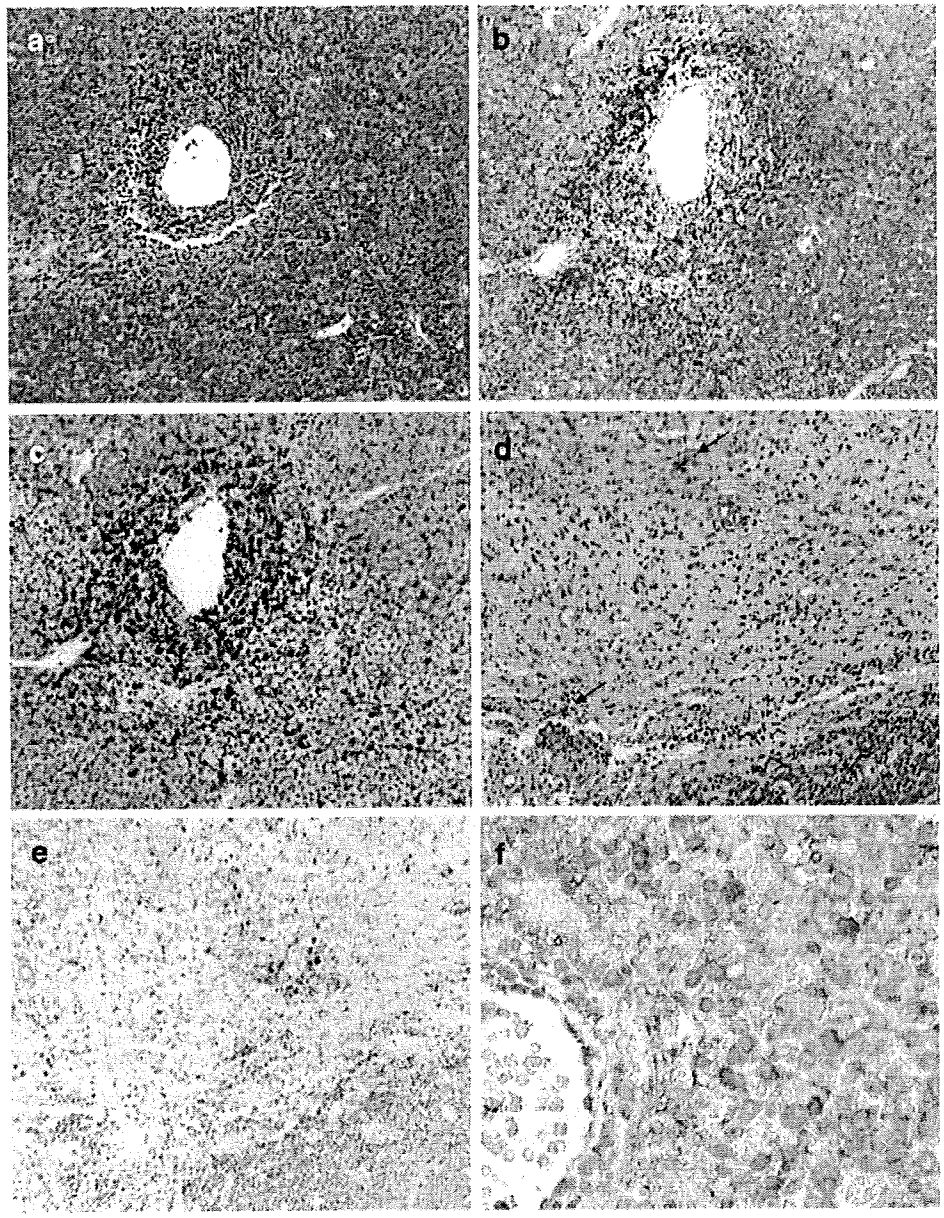


**Fig. 2.** Pathologic findings of the biopsy specimen obtained from left frontal lesion (a–f). a. Pathologic specimen of gadolinium-enhanced area shows hypercellular infiltration of malignant lymphocytes around cerebral blood vessels. Tumor cells were characterized by the variable cellular size and shape with large nuclei and mitotic figures (Hematoxylin-eosin, original magnification ×50). b. Immunohistochemical staining for L26. Majority of tumor cells positively stained with B-cell marker L26 (original magnification ×100). c. Immunohistochemical staining for UCHL-1. Reactive lymphocytes cerebral blood vessels positively stained with T-cell marker UCHL-1 (original magnification ×100). d. Pathologic specimen of hemorrhagic area shows slightly infiltration of malignant lymphocytes with hemosiderin deposits (arrows) (Hematoxylin-eosin, original magnification ×50). e. Numerous ion-reactive granules were defined by Perls's stain with Brazilian counterstain in hemorrhagic area (Perls's stain with Brazilian counterstain, original magnification ×50). f. Immunohistochemical staining of VEGF demonstrates the cytoplasmic or membrane of tumor cells were positive staining for anti-vascular endothelial growth factor antibody (original magnification ×200).

varied in size and shape with large nuclei and mitotic figures. Immunohistochemical studies showed that the majority of the tumor cells were positive for L26 antibody (B-cell marker; Fig. 2b) and some reactive lymphocytes were positive for UCHL-1 antibody (T-cell marker; Fig. 2c). These pathologic features were compatible with malignant lymphoma of diffuse large B-cell type. Moreover, the tumor cell cytoplasm and membrane stained positively for anti-vascular endothelial growth factor (VEGF) antibody (diluted 1:500, Thermo Fisher Scientific Anatomical Pathology, Kalamazoo, MI; Fig. 1f). Systemic staging evaluations, including ophthalmologic examination, spine MRI, and contrast enhanced computed tomography of the chest, abdomen, and pelvis were negative. Systemic and intrathecal chemotherapy began 3 days after surgery. Her neurologic symptoms gradually improved along with the disappearance of the gadolinium enhancement and a decrease in the size of the lesion on MRI.

## 3. Discussion

We describe a pathologically confirmed case of primary CNS lymphoma with cortical laminar hemorrhage on MRI. The present case showed an acute onset of focal neurologic signs and bilateral cerebral lesions in the left frontal and right parietal cortices surrounded by peripheral white matter edema on MRI. These cortical lesions presented the typical MRI findings of primary CNS lymphoma manifestations, such as hypercellularity with slight hyperintensity on T2-weighted images, dense enhancement, and close contact with the

leptomeningeal space [11–14]. Moreover, the subacute cortical laminar hemorrhage in a part of the left frontal cortical lesion was hyperintense on T1-weighted images and hypointense on T2-weighted and T2*-weighted gradient-echo images. Koeller et al. reported that only 7% of a series of 352 patients diagnosed with primary CNS lymphoma exhibited symptoms of ischemic stroke [11]. CNS lymphomas can infiltrate the brain as solitary lesions and as multiple mass lesions. Multiple mass lesions most often contact the ependymal and leptomeningeal space [3,11,12], and calcification, cyst formation, and hemorrhage are very rarely observed before treatment [15]. The atypical MRI finding of our case was the cortical hemorrhage. Therefore, the initial presumptive diagnosis was multiple hemorrhagic infarctions based on the acute onset of symptoms and MRI findings, but the pathologic diagnosis was compatible with diffuse large B-cell lymphoma.

Atypical course of CNS lymphoma may appear and may imitate other cerebral diseases, leading to severe diagnostic problems in daily clinical routine. 201-Tl-Chloride belongs to the group of unspecific tumor markers; its uptake depends on the Na/K-ATPase, which is mainly independent form cerebral blood flow and is probably associated with mitochondrial activity in tumor cells. So the high 201-Tl uptake in the lesions indicates a cerebral neoplasm rather than infarction. In contrast, uptake of Gadolinium contrast is caused by a disruption of the blood-brain-barrier (BBB), which is in case of lymphoma independent from tumor proliferation. Moreover, 201-Tl accumulation is observed in a variety of other cerebral diseases presenting with BBB breakdown [16]. DWI findings are helpful in differentiating lymphomas from other brain tumors [17]. Indeed, it can be difficult in some cases to distinguish lymphoma-caused DWI changes from cerebral infarction [18]. The main problem of lymphomas is that they appear similar to other cerebral diseases and it is therefore challenging to make the correct diagnosis, as in the presented case. These findings reconfirm that histologic examination following brain biopsy is necessary for a correct diagnosis of primary CNS lymphoma and suggest that this case adds to the MRI spectrum of primary CNS lymphoma for differential diagnosis.

The radiologic and neuropathologic findings in this case seemed to be consistent with each other; that is, the hypercellular area of the malignant lymphocytes caused high signal on DWI and low ADC values as well as the other typical MRI findings of primary CNS lymphoma. The MRI appearance of the cortical laminar hemorrhage was due to blood degradation products such as methemoglobin and hemosiderin. Histopathology revealed hemosiderin, the presence of which leads to hyperintensity on T1-weighted images and hypointensity on T2-weighted and T2*-weighted images. In general, the hypercellularity of cerebral tumors is responsible for hyperintense signal alterations on DWI and low ADC values [17]. Subacute hemorrhage appears hyperintense on T1-weighted images and hypointense on T2-weighted and T2*-weighted gradient-echo images [19,20]. Therefore, the MRI features of our case were conclusively consistent with the pathologic findings.

Hemorrhagic lesions in primary CNS lymphoma are extremely rare [6–9]. In the previous reports, two cases showed a small mass of hemorrhage and one case had a massive hematoma. The cortical laminar hemorrhage in the present case differed in appearance from the intratumoral hemorrhage in the previous cases. Although there are reports of intravascular lymphomatosis in cerebral infarctions in dogs and humans with intravascular lymphomatosis [21,22], the present case did not show the pathologic findings of intravascular lymphomatosis and ischemic stroke. Rubenstein et al. [6] reported a case of hemorrhagic primary CNS lymphoma with higher VEGF immunoreactivity and suggested that intense VEGF expression could contribute to vascular destabilization and permeability changes, vasogenic edema, and intracerebral hemorrhage in primary CNS lymphoma. They also reported that the presumptive pathogenic mechanisms of hemorrhage in the CNS lymphoma may be rapid growth and breakdown of vessels around the tumors caused by the overexpression of VEGF and matrix metalloproteinases from tumor cells [6]. Although the definitive mechanism of hemorrhage limited to the cerebral cortex is unclear, one possible explanation for this finding in our case may be, that the CNS lymphoma, which mainly involved the cortex, consisted some malignant lymphocytes, which were positive for VEGF, leading to infiltrations of vessel walls and finally to vessel disruptions. Thus, the immunohistochemical findings in the present case were consistent with those of Rubenstein et al. and support a possible correlation between intratumoral hemorrhage and VEGF expression in primary CNS lymphoma.

In summary, this is the first report of a case of primary CNS lymphoma with cortical laminar hemorrhage. Brain biopsy is a crucial procedure for the correct diagnosis of primary CNS lymphoma and appropriate treatment. The neuropathologic examination in this case suggests that VEGF expression is involved in spontaneous tumor hemorrhage in primary CNS lymphoma.

## References

[1] Bataille B, Delwail V, Menet E, Vandermarcq P, Ingrand P, Wager M, et al. Primary intracerebral malignant lymphoma: report of 248 cases. J Neurosurg 2000;92:261–6.
[2] Morgello S. Pathogenesis and classification of primary central nervous system lymphoma: an update. Brain Pathol 1995;5:383–93.
[3] Bhagavathi S, Wilson JD. Primary central nervous system lymphoma. Arch Pathol Lab Med 2008;132:1830–4.
[4] Trendelenburg G, Zimmer C, Forschler A, Stadelmann C, Zschenderlein R. Atypical appearance of a primary central nervous system lymphoma. Arch Neurol 2006;63:908–9.
[5] Giglio P, Bakshi R, Block S, Ostrow P, Pullicino PM. Primary central nervous system lymphoma masquerading as herpes encephalitis: clinical, magnetic resonance imaging, and pathologic findings. Am J Med Sci 2002;323:59–61.
[6] Rubenstein J, Fischbein N, Aldape K, Burton E, Shuman M. Hemorrhage and VEGF expression in a case of primary CNS lymphoma. J Neurooncol 2002;58:53–6.
[7] Fukui MB, Livstone BJ, Meltzer CC, Hamilton RL. Hemorrhagic presentation of untreated primary CNS lymphoma in a patient with AIDS. Am J Roentgenol 1998;170:1114–5.
[8] Kim IY, Jung S, Jung TY, Kang SS, Choi C. Primary central nervous system lymphoma presenting as an acute massive intracerebral hemorrhage: case report with immunohistochemical study. Surg Neurol 2008;70:308–11.
[9] Ueda F, Takashima T, Suzuki M, Kadoya M, Yamashita J, Kida T. MR imaging of primary intracranial malignant lymphoma. Radiat Med 1995;13:51–7.
[10] Castillo M, Scatliff JH, Kwock L, Green JJ, Suzuki K, Chancellor K, et al. Postmortem MR imaging of lobar cerebral infarction with pathologic and in vivo correlation. Radiographics 1996;16:241–50.
[11] Koeller KK, Smirniotopoulos JG, Jones RV. Primary central nervous system lymphoma: radiologic-pathologic correlation. Radiographics 1997;17:1479–526.
[12] Coulon A, Lafitte F, Hoang-Xuan K, Martin-Duverneuil N, Mokhtari K, Blustajn J, et al. Radiographic findings in 37 cases of primary CNS lymphoma in immunocompetent patients. Eur Radiol 2002;12:329–40.
[13] Jack Jr CR, Reese DF, Scheithauer BW. Radiographic findings in 32 cases of primary CNS lymphoma. Am J Roentgenol 1986;146:271–6.
[14] Roman-Goldstein SM, Goldman DL, Howieson J, Belkin R, Neuwelt EA. MR of primary CNS lymphoma in immunologically normal patients. Am J Neuroradiol 1992;13:1207–13.
[15] Jenkins CN, Colquhoun IR. Characterization of primary intracranial lymphoma by computed tomography: an analysis of 36 cases and a review of the literature with particular reference to calcification haemorrhage and cyst formation. Clin Radiol 1998;53:428–34.
[16] Hayashi T, Kumabe T, Jokura H, Fujihara K, Shiga Y, Watanabe M, et al. Inflammatory demyelinating disease mimicking malignant glioma. J Nucl Med 2003;44:565–9.
[17] Reiche W, Hagen T, Schuchardt V, Billmann P. Diffusion-weighted MR imaging improves diagnosis of CNS lymphomas. A report of four cases with common and uncommon imaging features. Clin Neurol Neurosurg 2007;109:92–101.
[18] Provenzale JM, Sorensen AG. Diffusion-weighted MR imaging in acute stroke: theoretic considerations and clinical applications. Am J Roentgenol 1999;173:1459–67.
[19] Ebisu T, Tanaka C, Umeda M, Kitamura M, Fukunaga M, Aoki I, et al. Hemorrhagic and nonhemorrhagic stroke: diagnosis with diffusion-weighted and T2-weighted echo-planar MR imaging. Radiology 1997;203:823–8.
[20] Siskas N, Lefkopoulos A, Ioannidis I, Charitandi A, Dimitriadis AS. Cortical laminar necrosis in brain infarcts: serial MRI. Neuroradiology 2003;45:283–8.
[21] Kent M, Delahunta A, Tidwell AS. MR imaging findings in a dog with intravascular lymphoma in the brain. Vet Radiol Ultrasound 2001;42:504–10.
[22] Holmøy T, Nakstad PH, Fredø HL, Kumar T. Intravascular large B-cell lymphoma presenting as cerebellar and cerebral infarction. Arch Neurol 2007;64:754–5.

# Clinical Investigative Study

# Evaluation of the Effects of Thyrotropin Releasing Hormone (TRH) Therapy on Regional Cerebral Blood Flow in the Cerebellar Variant of Multiple System Atrophy Using 3DSRT

**Noriyuki Kimura, PhD, Toshihide Kumamoto, MD, Teruaki Masuda, MD, Yuki Nomura, MD, Takuya Hanaoka, MD, Yusuke Hazama, MD, Toshio Okazaki, MD**

From the Department of Internal Medicine III, Oita University, Faculty of Medicine, Oita, Japan

## ABSTRACT

### BACKGROUND

**Thyrotropin releasing hormone (TRH) improves cerebellar ataxia and cerebellar perfusion in patients with spinocerebellar degeneration. It is not known whether TRH therapy can improve the cerebellar regional cerebral blood flow (rCBF) or not in patients with cerebellar variant of multiple-system atrophy (MSA-C).**

### PATIENTS AND METHODS

**Seven patients with MSA-C received TRH intravenously (2 mg/day) for 14 days. Clinical efficacy was assessed using the International Cooperative Ataxia Rating Scale (ICARS) and brain perfusion single photon emission-computed tomography was performed before and after therapy. The rCBF in each region of interest (ROI) was calculated using 3DSRT, a fully automated the ROI technique.**

### RESULTS

**The ICARS scores slightly improved in 6 of the 7 patients after TRH therapy, but this was not statistically significant. After TRH therapy, the cerebellar rCBF reduced in the 6 of 7 patients and the mean rCBF in cerebellum also significantly decreased ($P = 0.029$, paired $t$-test), whereas the rCBF in the precentral segment tend to increase ($P = 0.048$, paired $t$-test).**

### CONCLUSION

**TRH therapy may be less effective on cerebellar ataxia and cerebellar rCBF in MSA-C. The 3DSRT program may be useful for the evaluation of the efficacy of TRH therapy on cerebral blood flow.**

**Keywords:** Cerebellar variant of multiple system atrophy, thyrotropin releasing hormone, brain perfusion SPECT, regional cerebral blood flow, 3DSRT.

**Acceptance:** Received April 9, 2009, and in revised form June 24, 2009. Accepted for publication July 10, 2009.

**Correspondence:** Address correspondence to Noriyuki Kimura, PhD, Department of Internal Medicine III, Oita University, Faculty of Medicine, Idaigaoka 1-1, Hasama, Yufu, Oita 879-5593, Japan. E-mail: noriyuki@med.oita-u.ac.jp

J Neuroimaging 2009;XX:1-6.
DOI: 10.1111/j.1552-6569.2009.00411.x

## Introduction

Thyrotropin releasing hormone (TRH) regulates the release of thyrotropin from the pituitary gland. TRH also has neuroprotective effects as a neuromodulator or neurotransmitter in the brain,[1] and is therefore used as a therapeutic agent in cases of encephalitis, trauma,[2,3] brain ischemia,[4] and neurodegenerative disorders.[5,6] TRH administered intravenously at a dose of 2 mg/day for 14 days significantly improves cerebellar ataxia in patients with spinocerebellar degeneration (SCD).[7,8] Similarly, we previously reported that TRH therapy may increase cerebellar regional cerebral blood flow (rCBF) in some patients with cerebellar forms of SCD.[9] However, the efficacy of TRH therapy has been infrequently investigated in patients with cerebellar variant of multiple-system atrophy (MSA-C).[10] MSA-C is a sporadic progressive neurodegenerative disorder clinically characterized by predominantly cerebellar features with various combinations of parkinsonian, autonomic, and pyramidal symptoms or signs and has more progressive clinical course and a poor prognosis in comparison with cerebellar forms of SCD.[11,12] In this study, we evaluated the efficacy of TRH therapy based on clinical parameters and quantitative analysis of brain perfusion in the patients with MSA-C. The rCBF in 12 different brain regions was measured using the noninvasive Patlak plot method and calculated using 3DSRT both before and after 14 days of TRH therapy. The 3DSRT program allows for the objective assessment of rCBF by automatically setting the regions of interest (ROIs) based on anatomically standardized single photon emission-computed tomography (SPECT) images and is useful for the diagnosis of various neurodegenerative disorders and the evaluating the drug efficacy.[9,13-15] The aim of our study was to objectively determine the efficacy of TRH treatment in patients with MSA-C.

 

## Material and Methods

*Patients*

Patients with MSA-C admitted to the Department of Internal Medicine III at the Oita University from January 2006 to February 2009 were included in the study. The subjects were 7 patients with MSA-C (5 males and 2 females; age range 46–79 years; mean age 61.3). A diagnosis of MSA-C was made according to the consensus criteria proposed for probable and possible MSA.[16] Informed consent was obtained from all subjects or their closest relative. All patients received a neurologic examination and a diagnostic evaluation that included routine laboratory tests measuring the complete blood count, urine components, blood biochemistry, thyroid function, Vitamin E levels, and tumor markers. For radiologic examination, brain magnetic resonance imaging (MRI) and SPECT were performed in all patients. MRI was performed using a 1.5 T scanner. The spin-echo acquisition parameters were 3000-4500/90 (repetition time [TR]/echo time [TE]) for the T2-weighted axial images. The slice thickness was 5 mm with a 2.5-mm interval between successive slices. TRH (2 mg/day) was administered intravenously daily for 14 days. Clinical evaluation was recorded before and after treatment using the International Cooperative Ataxia Rating Scale (ICARS).[17] The same person assessed the ICARS for each patient, but could not be blinded to the treatment because healthy control subjects were not included in the study. The ICARS score was expressed as mean value ± standard deviation and compared between before and after TRH therapy.

*Brain SPECT Imaging*

SPECT was performed in all patients before and after TRH therapy. Patients were asked to maintain a comfortable supine position with eyes closed in quiet surroundings. After an injection of $^{99m}$Tc ethylcysteinate dimer (600 MBq, FUJIFILM RI Pharma Co., Ltd., Tokyo, Japan), its passage from the heart to the brain was monitored using a rectangular large field gamma camera (E. Cam Signature, Toshiba Medical, Tokyo, Japan). Ten minutes after the angiography, SPECT images were obtained using a rotating, dual-head gamma camera. Data were acquired as a sequence of 120 frames at a rate of 1 frame per second with a 128 × 128 matrix. All SPECT images were reconstructed using ramp-filtered back-projection and then 3-dimensionally smoothed with a Butterworth filter. The reconstructed images were corrected for gamma ray attenuation using the Chang method. For rCBF quantification, the noninvasive Patlak plot method[18,19] was used on a $^{99m}$Tc ethylcysteinate dimer cerebral blood flow perfusion SPECT. Quantitative flow-mapping images were obtained from the qualitative perfusion images using Patlak plot graphical analysis and Lassen's correction, as previously reported.[15,20,21] The rCBF in each ROI was calculated using the 3DSRT software, which is a fully automated ROI technique developed by Takeuchi et al.[13] The blood flow in each ROI was quantified as the value in milliliters per 100 g/min. These ROIs were categorized into 12 segments; the callosomarginal, precentral, central, parietal, angular, temporal, posterior cerebral, pericallosal, lenticular nucleus, thalamus, hippocampus, and cerebellum segments in the template, and the rCBF was expressed as the mean value ± standard deviation (SD) bilaterally for each segment.[13-15] The mean rCBF in all segments was compared between before and after TRH therapy. We also used an easy Z-score imaging system (eZIS) program to supplement the diagnosis and to detect a statistically significant decrease in blood perfusion. A Z-score map for each SPECT image was extracted from the comparison with the mean and SD of SPECT images of age-matched normal controls that had been incorporated into the eZIS program as a normal control database. A voxel-by-voxel Z score analysis was performed after voxel normalization to global means or cerebellar values; Z-score = ([control mean] − [individual value]/(control SD). These Z-score maps were displayed by overlaying them on tomographic sections and projecting the averaged Z-score of a 14-mm thickness-to-surface rendering of the anatomically standardized magnetic resonance (MR) imaging template.[22,23]

*Statistical Analysis*

The differences in the rCBF and ICARS before and after TRH therapy were analyzed using the paired *t*-test. In addition, the correlations between the change in rCBF in cerebellum as well as precentral segment and the disease duration, the ICARS scores at baseline and the improved ICARS scores after treatment were evaluated by regression analysis. A $P$ value of less than .05 was considered to be statistically significant.

## Results

Table 1 summarizes the clinical and demographic characteristics of the patients with MSA-C. The mean age was 61.3 ± 9.2 years and the mean disease duration at the time of TRH therapy was 3.0 ± 1.5 years. The baseline mean ICARS value was 36.4 ± 13.6 (range, 13–55), indicating high variability in the disease severity between patients. Brain MRI demonstrated various degrees of brain atrophy in the cerebellum and brainstem in all patients (Fig 1). The abnormal signal hyperintensity in the pontine base and middle cerebellar peduncles, which is characteristic of MSA, was clearly observed in 2 patients on T2-weighted MR images. The eZIS analysis revealed that rCBF was relatively decreased in the cerebellum and brainstem in all patients, compared with the normal values from the control data (Fig 2). Although the ICARS scores decreased in 6 of the 7 patients after TRH therapy, the degree of improvement was slight except for patient 4. The mean ICARS score also decreased from 36.4 ± 13.6 to 30.9 ± 13.9, but this was not statistically significant ($P$ = .212, paired *t*-test). The global CBF value increased in 3 of the 7 patients after TRH therapy; the change in global CBF value, however, was not significant ($P$ = 0.952, paired *t*-test). A comparison of the mean rCBF in each segment both before and after TRH treatment is shown in Table 2. The cerebellar rCBF value decreased in 6 of the 7 patients and the mean cerebellar rCBF value significantly decreased following TRH therapy ($P$ = .029, paired *t*-test). Decreased cerebellar rCBF tended to correlate inversely with baseline ICARS scores, but this was not statistically significant ($P$ = .095, regression analysis). The correlation between the change

Table 1. Summary of the Clinical and Demographic Characteristics in the Patients with MSA-C

| | Sex | Age (y) | Duration (y) | Diagnosis | ICARS | | Global CBF | | Cerebellar CBF | |
|---|---|---|---|---|---|---|---|---|---|---|
| | | | | | Before | After | Before | After | Before | After |
| Patient 1 | F | 66 | 3 | probable MSA | 35 | 34 | 38.5 | 36.6 | 32.1 | 31.3 |
| Patient 2 | M | 56 | 3 | probable MSA | 55 | 43 | 42.3 | 46.0 | 36.5 | 28.5 |
| Patient 3 | M | 62 | 1 | probable MSA | 41 | 48 | 38.1 | 40.8 | 40.1 | 36.6 |
| Patient 4 | F | 60 | 4 | probable MSA | 44 | 18 | 46.9 | 44.1 | 35.0 | 33.2 |
| Patient 5 | M | 46 | 2 | probable MSA | 46 | 44 | 39.8 | 36.3 | 43.5 | 35.4 |
| Patient 6 | M | 79 | 2 | probable MSA | 21 | 18 | 42.5 | 41.9 | 34.0 | 29.6 |
| Patient 7 | M | 60 | 6 | probable MSA | 13 | 11 | 38.5 | 41.4 | 38.6 | 39.5 |

M = male; F = female; Duration = disease duration; y = year; ICARS = International Cooperative Ataxia Rating Scale; Global CBF = mean value of the cerebral blood flow in the bilateral cerebral hemisphere before and after therapy (milliliters per 100 g/min). Cerebellar rCBF = mean value of the cerebral blood flow in the bilateral cerebellum before and after therapy (milliliters per 100 g/min).

in cerebellar rCBF value and age, disease duration, or improved ICARS scores was not significant ($P = .375$, $P = .160$, and $P = .969$, respectively; regression analysis). The mean rCBF value increased in the precentral segment after TRH treatment ($P = .048$, paired $t$-test). The increased mean rCBF value was also observed in the callosomarginal, precentral, central, angular, temporal, pericallosal segments and thalamus, but this was not statistically significant. Although the 5 of the 6 patients with improved ICARS scores had increased rCBF in the precentral segment (Fig 3), the correlation between the change in rCBF

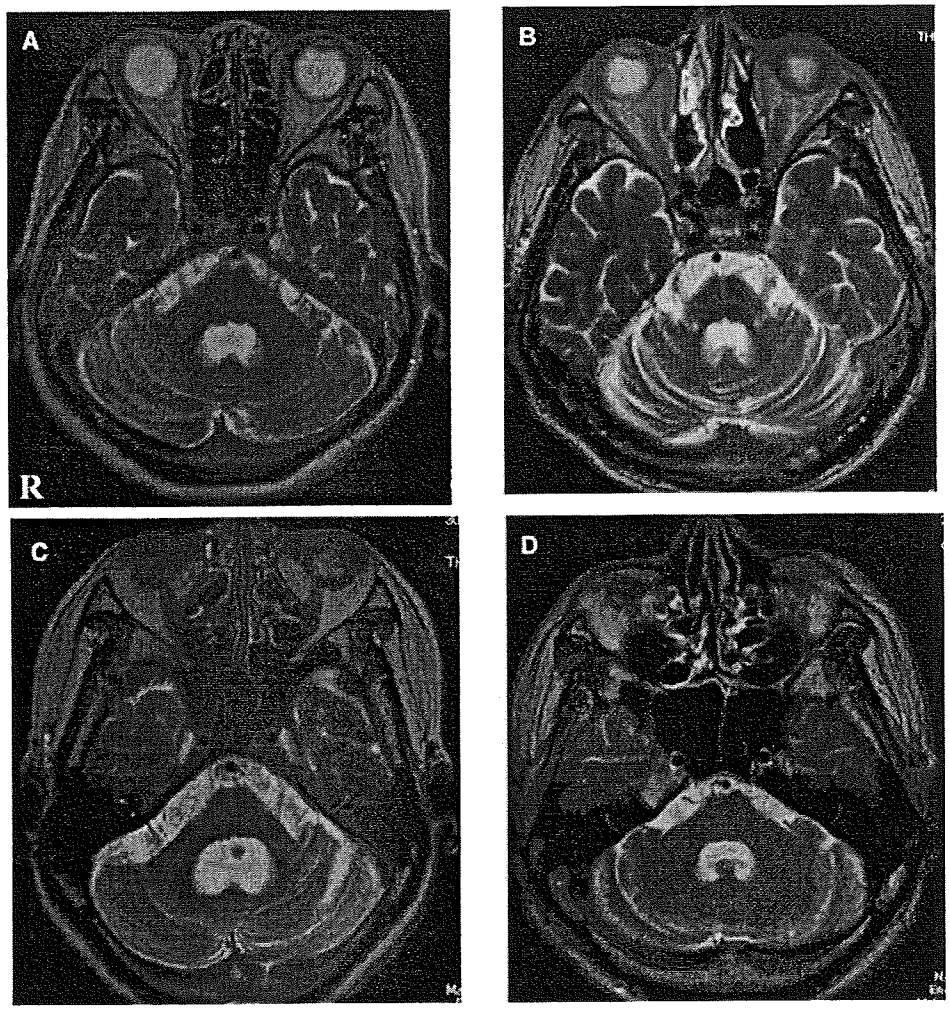


**Fig 1.** T2-weighted MR images (axial images) in patients with MSA-C. The various degrees of brain atrophy were observed in the cerebellum, pons, and middle cerebellar peduncles. Cerebellar atrophy with brainstem involvement was mild in patients 1 (A) and 7 (D), moderate in patient 4 (C), and severe in patient 2 (B). Abnormal signal hyperintensity in the pontine base was clearly observed in patient 2 (B).

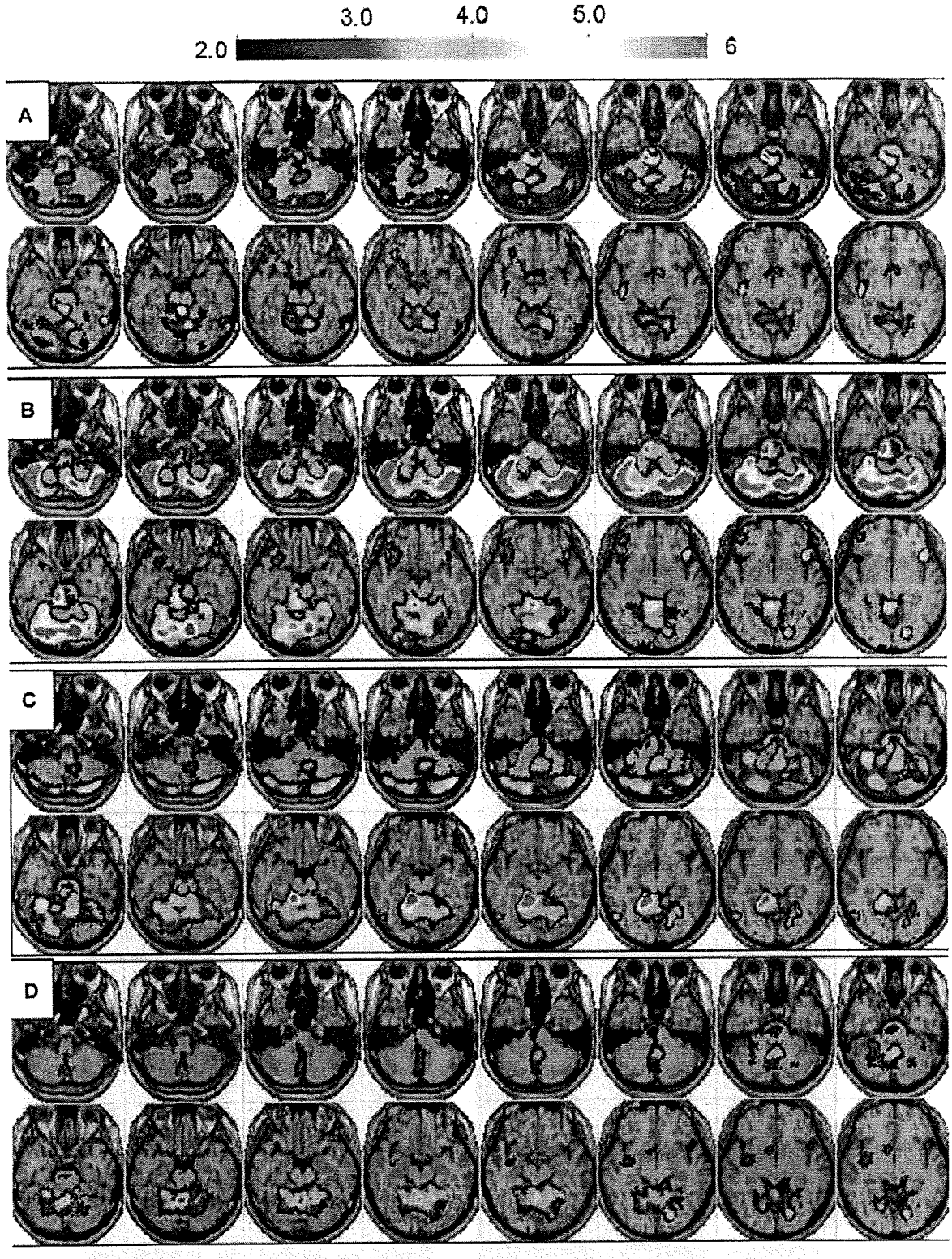


**Fig 2.** eZIS images (axial view) in patients with MSA-C. The color images represent the statistical significance (Z-score) of the decrease in rCBF. The relative rCBF reduction was detected in the cerebellum and pons in all patients. The relative rCBF reduction in the cerebellum was significant, but mild in patients 1 (A) and 7 (D), moderate in patients 4(C), and severe in patient 2 (B).

Table 2. Regional Cerebral Blood Flow (rCBF) before and after TRH Therapy Calculated Using 3DSRT. The rCBF is Expressed as Mean ± SD (milliliter per 100 g/min)

| Region | rCBF (before) | rCBF (after) | *P* value |
|---|---|---|---|
| Callosomarginal | 39.07 ± 4.44 | 40.24 ± 4.73 | .347 |
| Precentral | 38.84 ± 3.60 | 41.70 ± 3.32 | .048* |
| Central | 36.40 ± 3.63 | 38.63 ± 3.47 | .183 |
| Pariental | 38.44 ± 2.85 | 35.44 ± 2.19 | .091 |
| Angular | 38.02 ± 2.41 | 39.03 ± 2.64 | .48 |
| Temporal | 35.31 ± 3.32 | 35.85 ± 2.92 | .637 |
| Occipital | 38.66 ± 1.67 | 38.64 ± 2.13 | .785 |
| Pericallosal | 39.11 ± 3.40 | 40.60 ± 3.71 | .209 |
| Lenticularnucleus | 40.97 ± 5.54 | 40.16 ± 6.06 | .881 |
| Thalamus | 38.24 ± 6.85 | 40.53 ± 7.42 | .216 |
| Hippocampus | 29.99 ± 3.08 | 29.47 ± 3.37 | .907 |
| Cerebellum | 36.85 ± 3.89 | 32.42 ± 3.96 | .030* |

rCBF = mean value of regional cerebral blood flow bilaterally in each segment.

value and the improved ICARS score was not significant ($P$ = .981; regression analysis).

## Discussion

We performed the quantitative analyses of the rCBF in each ROI before and after TRH intravenous administration at a dose of 2 mg/day for 14 days to evaluate the efficacy of TRH treatment in patients with MSA-C. Although manual quantitative measurements of rCBF have been used to assess the effects of TRH, the reproducibility and objectivity of the results are problematic.[3,24] We measured automatically and objectively the rCBF in each ROI using a fully automated ROI technique,

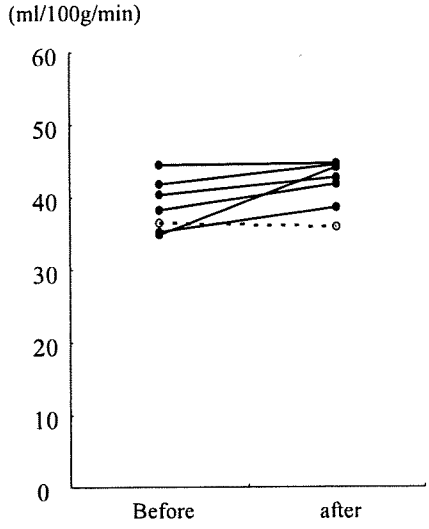


**Fig 3.** Cerebral blood flow before and after TRH therapy calculated using 3DSRT. The rCBF in the precentral segment increased in 6 patients and decreased in 1 patient. The mean values of rCBF were significantly increased ($P$ = .048, paired $t$-test). ●; patient with increased cerebellar rCBF, ○; patient with stable or decreased cerebellar rCBF.

3DSRT. All the patients demonstrated various degrees of atrophy in the brainstem and middle cerebellar peduncles and 2 patients had a clear "hot cross bun" sign in pontine base on the MR images. The eZIS analysis revealed a relative decrease of rCBF in the cerebellum and brainstem in all patients compared to the control data, consistent with the results of previous studies.[22]

TRH therapy slightly improved the ICARS scores in 6 of the 7 patients, but this was not statistically significant. The cerebellar rCBF reduction was observed in 6 of 7 patients and the mean rCBF in cerebellum also significantly decreased. The degree of cerebellar rCBF reduction tended to be more severe in patients with severe disability than in those with mild disability. Previous human studies on TRH therapy reported an increased CBF in the cerebrum in cases of viral encephalopathy and SCD.[3,24] Similarly, we reported that TRH therapy significantly improved cerebellar ataxia and cerebellar rCBF in patients with cerebellar form of SCD and suggested that the beneficial effects of TRH may be due to increased cerebellar rCBF.[9] Therefore, our results suggest that TRH therapy may be less effective against cerebellar ataxia and cerebellar rCBF in MSA-C compared to the cerebellar form of SCD. The refractory nature of MSA-C to TRH therapy may be due to the different distributions and severity of neuronal degeneration between MSA-C and cerebellar form of SCD, because the pathologic changes are widely and severely detected in olivopontocerebellar region, striatonigral region, and autonomic nervous system in MSA-C,[11,12,25] whereas those are mainly limited to the cerebellar cortex and inferior olivary nucleus in cerebellar form of SCD.[26] The mechanism underlying the TRH-induced increase in rCBF is thought to involve cerebral vasodilatation, which is mediated by the intrinsic cholinergic system in the brainstem.[27,28] MSA-C shows the decreased levels of neurotransmitter metabolites in cerebral spinal fluid[29,30] and the rCBF reduction in the brainstem as well as cerebellum.[9,22,31] Therefore, we speculate that the widespread involvement in the central nervous system, particularly brainstem, may contribute to the cerebellar rCBF reduction, which corresponds to the lack of a significantly improved ICARS scores in patients with MSA-C.

Our results also showed that 6 of the 7 patients tended to show increased rCBF in the precentral segment after TRH therapy. Although our findings do not indicate a significant correlation between the change in rCBF and improved ICARS scores, 5 of the 6 patients with slightly improved ataxic symptoms had increased rCBF in the precentral segment. One possible explanation for this finding might be that increased rCBF in the precentral segment may be related to the slightly improved ataxic symptoms in MSA-C because there is an extensive anatomic connection between the cerebellum and the frontal and parietal lobes.[32] Alternatively, the increased rCBF in the precentral segment may be a secondary effect of TRH therapy.

There are several limitations to this study. The number of patients with MSA-C was relatively small and we were unable to measure the effects of TRH on blood perfusion in healthy subjects for a control group. Further studies with bigger samples, including normal control groups, are needed to confirm our results.

In conclusion, a relative decrease of rCBF was observed in the brainstem and cerebellum in all patients with MSA-C. TRH therapy may be less effective against cerebellar ataxia and cerebellar rCBF in MSA-C. Brain perfusion analyzing programs, such as eZIS and 3DSRT, may be useful for the prediction and evaluation of the efficacy of TRH therapy.

## References


1. Morley JE. Extrahypothalamic thyrotropin releasing hormone (TRH) - its distribution and its functions. *Life Sci* 1979;25:1539-1550.
2. Tanaka K, Ogawa N, Asanuma M, et al. Thyrotropin releasing hormone prevents abnormalities of cortical acetylcholine and monoamines in mice following head injury. *Regul Pept* 1997;18:173-178.
3. Yoshinari S, Hamano S, Tanaka M, et al. Alteration of regional cerebral blood flow to thyrotropin-releasing hormone therapy in acute encephalitis and encephalopathy during childhood. *Eur J Paediatr Neurol* 2006;10:124-128.
4. Nakamura R, Fujita M. Effect of thyrotropin-releasing hormone (TRH) on motor performance of hemiparetic stroke patients. *Tohoku J Exp Med* 1990;160:141-143.
5. Luo L, Yano N, Mao Q, et al. Thyrotropin releasing hormone (TRH) in the hippocampus of Alzheimer patients. *J Alzheimers Dis* 2002;4:97-103.
6. Takeuchi Y, Miyanomae Y, Komatsu H, et al. Efficacy of thyrotropin-releasing hormone in the treatment of spinal muscular atrophy. *J Child Neurol* 1994;9:287-289.
7. Sobue I, Yamamoto H, Konagaya M, et al. Effect of thyrotropin-releasing hormone on ataxia of spinocerebellar degeneration. *Lancet* 1980;1:418-419.
8. Sobue I, Takayanagi T, Nakanishi T, et al. Controlled trial of thyrotropin releasing hormone tartrate in ataxia of spinocerebellar degenerations. *J Neurol Sci* 1983;61:235-248.
9. Kimura N, Kumamoto T, Masuda T, et al. Evaluation of the effect of thyrotropin releasing hormone (TRH) on regional cerebral blood flow in spinocerebellar degeneration using 3DSRT. *J Neurol Sci* 2009;281:93-98.
10. Waragai M, Ogawara K, Takaya Y, et al. Efficacy of TRH-T for spinocerebellar degeneration–the relation between clinical features and effect of TRH therapy. *Rinsho Shinkeigaku* 1997;37:587-594.
11. Yabe I, Soma H, Takei A, et al. MSA-C is the predominant clinical phenotype of MSA in Japan: analysis of 142 patients with probable MSA. *J Neurol Sci* 2006;249:115-121.
12. Watanabe H, Saito Y, Terao S, et al. Progression and prognosis in multiple system atrophy: an analysis of 230 Japanese patients. *Brain* 2002;125:1070-1083.
13. Takeuchi R, Sengoku T, Matsumura K. Usefulness of fully automated constant ROI analysis software for the brain: 3DSRT and FineSRT. *Radiat Med* 2006;24:538-544.
14. Tateno M, Utsumi K, Kobayashi S, et al. Usefulness of a blood flow analyzing program 3DSRT to detect occipital hypoperfusion in dementia with Lewy bodies. *Prog Neuropsychopharmacol Biol Psychiatry* 2008;32:1206-1209.
15. Tateno M, Kobayashi S, Utsumi K, et al. Quantitative analysis of the effects of donepezil on regional cerebral blood flow in Alzheimer's disease by using an automated program, 3DSRT. *Neuroradiol* 2008;50:723-727.
16. Gilman S, Low PA, Quinn N, et al. Consensus statement on the diagnosis of multiple system atrophy. *J Neurol Sci* 1999;163:94-98.
17. Trouillas P, Takayanagi T, Hallett M, et al. International Cooperative Ataxia Rating Scale for pharmacological assessment of the cerebellar syndrome. The Ataxia Neuropharmacology Committee of the World Federation of Neurology. *J Neurol Sci* 1997;145:205-211.
18. Matsuda H, Tsuji S, Shuke N, et al. Noninvasive measurements of regional cerebral blood flow using technetium-99m hexamethylpropylene amine oxime. *Eur J Nucl Med* 1993;20:391-401.
19. Matsuda H, Yagishita A, Tsuji S, et al. A quantitative approach to technetium-99m ethyl cysteinate dimer: a comparison with technetium-99m hexamethylpropylene amine oxime. *Eur J Nucl Med* 1995;22:633-637.
20. Lassen NA, Andersen AR, Friberg L, et al. The retention of [99mTc]-d,l-HM-PAO in the human brain after intracarotid bolus injection: a kinetic analysis. *J Cereb Blood Flow Metab* 1988;8:13-22.
21. Friberg L, Andersen AR, Lassen NA, et al. Retention of 99mTc-bicisate in the human brain after intracarotid injection. *J Cereb Blood Flow Metab* 1994;14:19-27.
22. Waragai M, Yamada T, Matsuda H. Evaluation of brain perfusion SPECT using an easy Z-score imaging system (eZIS) as an adjunct to early-diagnosis of neurodegenerative diseases. *J Neurol Sci* 2007;260:57-64.
23. Matsuda H, Mizumura S, Nagao T, et al. Automated discrimination between very early Alzheimer disease and controls using an easy Z-score imaging system for multicenter brain perfusion single-photon emission tomography. *AJNR Am J Neuroradiol* 2007;28:731-6.
24. Izumi Y, Fukuuchi Y, Ishihara N, et al. Effect of thyrotropin-releasing hormone (TRH) on cerebral blood flow in spinocerebellar degeneration and cerebrovascular disease. *Tokai J Exp Clin Med* 1995;20:203-208
25. Ozawa T, Paviour D, Quinn NP, et al. The spectrum of pathological involvement of the striatonigral and olivopontocerebellar systems in multiple system atrophy: clinicopathological correlations. *Brain* 2004;127:2657-2671.
26. Ota S, Tsuchiya K, Anno M, et al. Distribution of cerebello-olivary degeneration in idiopathic late cortical cerebellar atrophy: clinicopathological study of four autopsy cases. *Neuropathology* 2008;28:43-50
27. Koskinen LO, Bill A. Thyrotropin-releasing hormone (TRH) causes sympathetic activation and cerebral vasodilation in the rabbit. *Acta Physiol Scand* 1984;122:127-136.
28. Koskinen LO. Effects of TRH on cerebral and peripheral blood flows; role of submesencephalic brain stem centres. *Acta Physiol Scand* 1986;128:277-288.
29. Abdo WF, van de Warrenburg BP, Munneke M, et al. CSF analysis differentiates multiple-system atrophy from idiopathic late-onset cerebellar ataxia. *Neurology* 2006;67:474-479.
30. Polinsky RJ, Brown RT, Burns RS, et al. Low lumbar CSF levels of homovanillic acid and 5-hydroxyindoleacetic acid in multiple system atrophy with autonomic failure. *J Neurol Neurosurg Psychiatry* 1988;51:914-919.
31. Cilia R, Marotta G, Benti R, et al. Brain SPECT imaging in multiple system atrophy. *J Neural Transm* 2005;112:1635-1645.
32. Rouiller EM, Liang F, Babalian A, et al. Cerebellothalamocortical and pallidothalamocortical projections to the primary and supplementary motor cortical areas: a multiple tracing study in macaque monkeys. *J Comp Neurol* 1994;345:185-213.

International Immunopharmacology 9 (2009) 366–370

Contents lists available at ScienceDirect

International Immunopharmacology

journal homepage: www.elsevier.com/locate/intimp

# Improvement of deficient natural killer activity and delayed bactericidal activity by a thiol proteinase inhibitor, E-64-d, in leukocytes from Chediak–Higashi syndrome patients *in vitro*

Fuminori Tanabe [a,*], Hirotake Kasai [b], Limin He [b], Tomohiro Kin [c], Takashi Fujikado [d], Toshihide Kumamoto [e], Toshiro Hara [f], Tsutomu Iwata [g], Masahiko Ito [b]

[a] Department of Human Science, Faculty of Medicine, Interdisciplinary Graduate School of Medicine and Engineering, University of Yamanashi, 1110 Shimokato, Chuo, Yamanashi 409-3898, Japan
[b] Department of Microbiology, Faculty of Medicine, Interdisciplinary Graduate School of Medicine and Engineering, University of Yamanashi, Yamanashi, Japan
[c] Suita Municipal Hospital, Suita, Japan
[d] Department of Applied Visual Science, Osaka University Medical School, Suita, Japan
[e] Department of Internal Medicine 3, Faculty of Medicine, Oita University, Oita, Japan
[f] Department of Pediatrics, Graduate School of Medical Sciences, Kyushu University, Fukuoka, Japan
[g] Department of Child Health and Development, Tokyo Kasei University, Tokyo, Japan

ARTICLE INFO

*Article history:*
Received 7 December 2008
Received in revised form 12 January 2009
Accepted 12 January 2009

*Keywords:*
Chediak–Higashi syndrome
Natural killer activity
Protein kinase C
Bactericidal activity

ABSTRACT

We previously reported that administration of a potent calpain inhibitor, E-64-d, which protects protein kinase C (PKC) from proteolysis, in a mouse model of Chediak–Higashi syndrome (CHS) (beige mice), decreases its susceptibility to *Staphylococcus aureus* infection. In the present study, we examined the *in vitro* effect of E-64-d on both deficient natural killer (NK) and delayed bactericidal activities of leukocytes from six CHS patients. Our results showed that pretreatment of peripheral blood mononuclear cells (PBMCs) obtained from CHS patients with E-64-d (1 μg/ml) significantly enhanced NK activity against K562 cells. The delayed bactericidal activity of polymorphonuclear cells (PMNs) against *S. aureus* also showed marked improvement. This was recovered to almost normal levels when PMNs were pretreated with E-64-d (1 μg/ml). On the other hand, the same concentration of E-64-d did not affect either the NK or bactericidal activity of normal controls. In addition, we confirmed that following E-64-d treatment, the abnormal down-regulation of PKC activity after concanavalin A (Con A) stimulation was eliminated in PBMCs obtained from CHS patients. To examine whether PKC is involved in the NK cell-mediated cytolysis and bactericidal activity of PMNs, two potent PKC inhibitors, chelerythrin and GÖ6976, were used. We found that chelerythrin inhibits NK activity of normal PBMCs in a dose-dependent manner, and GÖ6976 inhibits NK activity at doses that inhibit $Ca^{2+}$-dependent PKC isozymes. These inhibitors also suppressed the bactericidal activity of PMNs against *S. aureus*. Taken together, our findings suggested that E-64-d improved the compromised NK and bactericidal activity of leukocytes from CHS patients by reversing the down-regulation of PKC activity.



## 1. Introduction

Chediak–Higashi syndrome (CHS) is a rare autosomal recessive disorder that is accompanied by severe symptoms including immunological defects, and is characterized by partial oculocutaneous albinism and the presence of giant granules in several cell types [1–4]. It is known that natural killer (NK) activity and bactericidal activity are compromised in leukocytes isolated from CHS patients. Consequently, these individuals succumb to frequent pyogenic infections, principally from gram-positive bacteria such as *Staphylococcus aureus*, and associated lymphoproliferative disorders. Most CHS patients die young, unless they undergo a bone marrow transplant.

Human CHS is associated with mutations in *CHS 1*, a gene encoding for a cytosolic protein of 430 kDa. The same gene is responsible for the mouse beige mutation [5–7]. While the exact role of CHS 1 has not been elucidated, it was suggested that the CHS 1 protein regulates lysosomal fission [8] or affects cellular events such as that of nuclear phosphatidylinositol 4,5 biphosphate [9].

We previously reported that protein kinase C (PKC) activity is abnormally down-regulated after stimulation with phorbol ester or concanavalin A (Con A) in polymorphonuclear leukocytes (PMNs), NK cells, and fibroblasts from beige mice [10–12]. This aberrant down-regulation of PKC was caused by the enhanced calpain-mediated proteolysis of PKC, and was shown to be responsible for the impaired cellular functions observed in CHS patients. Calpain is a $Ca^{2+}$-dependent thiol proteinase and responsible for processing PKC into its inactive form [13]. We also reported that potent calpain inhibitors such as E-64-d

* Corresponding author.
*E-mail address:* ftanabe@yamanashi.ac.jp (F. Tanabe).

1567-5769/$ – see front matter © 2009 Elsevier B.V. All rights reserved.
doi:10.1016/j.intimp.2009.01.003